

Impulsive Fluidization of a Bi-Disperse Mixture in an Expanding Volume

by

Michael Giles Wisnewski

Submitted to the Department of Mechanical Engineering
in partial fulfillment of the requirements for the degree of

Master of Science in Mechanical Engineering

at the

MASSACHUSETTS INSTITUTE OF TECHNOLOGY

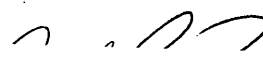
February 1994

© Massachusetts Institute of Technology 1994. All rights reserved.

Author

Department of Mechanical Engineering

January 31, 1994



Certified by

Carl R. Peterson

Associate Professor of Mechanical Engineering

Thesis Supervisor



Accepted by

Ain A. Sonin

Chairman, Departmental Committee on Graduate Students



MAR 08 1994

Impulsive Fluidization of a Bi-Disperse Mixture in an Expanding Volume

by

Michael Giles Wisnewski

Submitted to the Department of Mechanical Engineering
on January 31, 1994, in partial fulfillment of the
requirements for the degree of
Master of Science in Mechanical Engineering

Abstract

The motivation of this research program is to explore a design concept, incorporating crushing and material transport working together in a cyclical process, leading to improved comminution efficiencies. In simulating the comminution device, an experimental investigation is performed on the fluidized mechanical segregation process.

The experiments are performed in a plexiglass rectangular test section filled with a uniformly mixed bi-disperse mixture of particle sizes 0.2 mm and 3.0 mm in diameter. The mixture is subject simultaneously to an upward impulsive flow and an outwardly expanding wall motion. The experimental parameters varied are Inlet Flow Rate, Q_{li} , and Wall Velocity, V_w , as they are the most important in defining the fluidized mechanical segregation process. A field of 18 combinations of Q_{li} and V_w values (ranging from $Q_{li} = 2500 - 36,000 \text{ mm}^3/\text{s}$ and $V_w = 0 - 8.5 \text{ mm/s}$) is explored. This field of tests which cover a wide range of physical phenomena, is used as a template for addressing three design criterion. The three are (1) a Clearing Speed, final bed height divided by a process time, h_f/t_{pr} , (2) Fines Removal Fraction at process time, t_{pr} , and (3) Maximum Segregation Process Height. Three dimensional plots for each of these dependent variables with independent variables of Final Superficial Fluid Velocity (Inlet Flow Rate divided by final test section cross-sectional area, Q_{li}/A_f) and Wall Velocity (V_w) are created. Conclusions from these are that increased Wall Velocity improves Clearing Speed more strongly than increased Inlet Flow Rate. A higher Clearing Speed means more cycles of the crushing machine may be run in a shorter time. Fines Removal Fraction is more dependent on Inlet Flow Rate than on Wall Velocity, suddenly increasing at a Final Superficial Fluid Velocity (Q_{li}/A_f) corresponding to the terminal velocity of the fine particles. The Maximum Height in some of the 18 tests was the original bed height. This minimum clearance height translates into a smaller, cheaper crushing device. Lastly, the combination of the highest Inlet Flow Rate and Wall Velocity satisfies the three design criteria the best.

Thesis Supervisor: Carl R. Peterson

Title: Associate Professor of Mechanical Engineering

Acknowledgments

Without the help of a number of people, this work would not have been possible. My advisor, Professor Carl R. Peterson, has provided the necessary technical guidance, inspirational force, and financial backing to complete this work. Professors Harri K. Kytomaa and Frank A. McClintock have also been important contributors in the comminution project. The interactions with these three, plus with graduate student, Stefano Schiaffino, have been important and helpful in learning and progressing in the research project. Next, I thank Dick Fenner for his assistance and ideas in the design and construction of my experimental test section.

The two years in the MIT Fluid Mechanics Lab have been challenging, interesting and enjoyable. Having the diverse group of students there to associate with has been only a beneficial experience. I wish them good luck in their future endeavors. I also have others at MIT to thank, mostly for personal growth and a social life: Dr. Stephanie Gajar, Dr. Darryl Willoughby, Vicki Afshani, members of the Ashdown Intramural B-league Championship Softball team, and some from TCC. Lastly, I thank my family (Mom, Dad, Kate, and Jen). Without their constant support, none of this would have been possible.

Contents

1	Background and Motivation	10
1.1	Overview of Comminution Processes	11
1.1.1	Primary Crushing	11
1.1.2	Secondary, Tertiary and Quaternary Crushing	13
1.1.3	Fine Grinding	15
1.2	The New Design Concept	15
1.2.1	Material Transport	15
1.2.2	Proposed Machine Concept	16
1.3	Previous Work in Comminution Program: Particle Fracture in Beds .	18
1.4	Previous Work in Comminution Program: Particle Fluidization/Segregation	23
1.4.1	Steady Fluidization of Fine Particles Within a Coarse Matrix	23
1.4.2	Impulsive Fluidization of a Bi-Disperse Mixture	29
2	Impulsive Segregation of a Bi-Disperse Mixture Between Outwardly Moving Walls	38
2.1	Overview of Experimentation	38
2.1.1	Events Occuring in Time	39
2.1.2	Measured Results	41
2.2	Experimental Apparatus	43
2.2.1	Positive Displacement Device	43
2.2.2	Test Section Design and Construction	43
2.2.3	Movable Wall with Timing Belts and Pulleys	49
2.3	Experimental Measurement Tools	49

2.3.1	Image Analysis System	49
2.3.2	Luminance vs. Fines Concentration Calibration Curve for Minimum and Maximum Test Section Thicknesses	53
2.4	System Characterization: Step Wall and Step Flow Tests	54
2.5	Seven Experimental Parameters	57
2.6	Data Collection: Experimental Planar Plot	59
2.7	Results and Discussion	64
2.7.1	Qualitative Discussion of the Physical Phenomenon in the 13 Tests	64
2.7.2	Clearing Speed	66
2.7.3	Fines Removal Fraction at t_{pr}	73
2.7.4	Maximum Height of Process	75
2.7.5	Best Operating Point: 13	77
3	Conclusions	78
3.1	Summary	78
3.1.1	Impulsive Segregation of a Bi-Disperse Mixture Between Outwardly Moving Walls	79
3.2	Future Work	79
A	Dimensioned Plexiglass Test Section and Movable Wall	81
	Bibliography	84

List of Figures

1-1	Jaw Crusher (picture scanned from Cummins & Given, 1973).	12
1-2	Gyratory Crusher (picture scanned from Cummins & Given, 1973). .	12
1-3	Impact Crusher: Hammer Mill (picture scanned from Cummins & Given, 1973).	13
1-4	Cone Crusher (picture scanned from Mular & Bhappu, 1980).	14
1-5	Ball Mill (picture scanned from Mular & Bhappu, 1980).	15
1-6	Simplified Crushing-Transport Model	17
1-7	Conical Crushing Geometry	19
1-8	Fracture efficiency as a function of compression for 1 inch bed.	21
1-9	Typical stress-strain curve for 1 inch bed (30% compression).	21
1-10	Peak fracture efficiency as a function of compression for 1 inch bed. .	22
1-11	Experimental results for fluidization of 0.15 mm particles in a coarse bed.	26
1-12	Experimental results for fluidization of 0.2 mm particles in a coarse bed.	26
1-13	Experimental results for fluidization of 0.3 mm particles in a coarse bed.	27
1-14	Experimental results for fluidization of 0.4 mm particles in a coarse bed.	27
1-15	Sequence of video images spaced 1/6th of a second of an impulsively fluidized mixture of 0.2 mm fine and 4.0 mm coarse particles.	30
1-16	Measured quantities in impulsive fluidization tests.	33
1-17	Upward Bed Velocity.	34
1-18	Depletion Velocity of the rising plug, as measured by an observer moving with the same velocity of the plug (U_t).	34
1-19	Segregation speed.	35

1-20	Non-dimensional critical height. Data are grouped according to non-dimensional initial bed height.	36
1-21	Fine particle removal.	37
2-1	Sequence of Video Images (spaced 1/6th second). $Q_{li} = 11,000 \text{ mm}^3/\text{s}$, $V_w = 3.0 \text{ mm/s}$	40
2-2	Time History.	42
2-3	Experimental Apparatus.	44
2-4	Cylinder Calibration.	45
2-5	Test Section: front and side views.	46
2-6	Test Section Wall Halves.	47
2-7	Test Section Holder.	48
2-8	Pulley and No-Slip Belt System and Driving Mechanism for Movable Wall.	50
2-9	Wall Velocity Calibration.	51
2-10	Schematic of the image analysis system.	52
2-11	Luminance vs. Fines Concentration Calibration Curve for Minimum and Maximum Test Section Thicknesses.	54
2-12	Step Flow and Step Wall Motion.	55
2-13	Experimental Planar Plot.	60
2-14	Point 3: Low $V_w = 2.0 \text{ mm/s}$, High $Q_{li} = 36,000 \text{ mm}^3/\text{s}$. (frames spaced 1/6th second).	61
2-15	Point 6: High $V_w = 4.5 \text{ mm/s}$, Low $Q_{li} = 2500 \text{ mm}^3/\text{s}$. (frames spaced 1/6th second).	62
2-16	Clearing Speed, h_f/t_{pr}	67
2-17	Depletion Velocity of Plug.	68
2-18	Fluid Velocity for Point 10: $Q_{li} = 27,000 \text{ mm}^3/\text{s}$, $V_w = 6.5 \text{ mm/s}$	70
2-19	Control Volume for Fluid Velocity Analysis.	70
2-20	Path of Fluid Particle for Point 10: $Q_{li} = 27,000 \text{ mm}^3/\text{s}$, $V_w = 6.5 \text{ mm/s}$	72
2-21	Events Occuring in Time.	73

2-22 Fines Removal Fraction at t_{pr}	74
2-23 Maximum Height of Process.	76

List of Tables

1.1	Least square fitting of fluidization experimental data in log-log representation (Figs. 1-11 to 1-14).	28
1.2	Summary of test conditions for impulsive fluidization tests.	31
1.3	Geometrical dimensions of the three test sections used for impulsive fluidization.	31
2.1	Seven Experimental Parameters	58

Chapter 1

Background and Motivation

Comminution, the reduction of material to smaller pieces, is an industrial process seen in mining, food processing, and pharmaceuticals for example. Current comminution processes are major energy consumers: 2% of all U.S. electric power generation is used for comminution, 5% worldwide. Also, unfortunately, the processes are inefficient. Typical efficiency values range from 1-2%, with that energy input not going into comminution of feed material lost instead to noise, heat, and machine wear. There are many types of comminution devices in industry. The type this Comminution Program is interested in is one which crushes material in a bed between converging-diverging walls. Here, it is expected that upon crushing a bed of uniformly sized particles, a range of sizes will result. This means that multiple contact points between particles will be present upon compressive loading of the load. It is known that distribution of external loads among multiple contacts “blunts” the crushing action - hence there is a need to effectively remove small particles as they are formed. Selective removal of the fine material from the mixture can be achieved through upward liquid fluidization (material transport) because smaller particles are fluidized at lower fluid velocities than those necessary for larger particles. What is sought in this Comminution Program is an understanding of a machine incorporating crushing and material transport working together in a cyclical process which would lead to improved comminution efficiencies. The cycle refers to the cyclic converging-diverging of the walls. This study focuses on that period of time between the start of fine particle removal

from the mixture by way of impulsive fluidization to the beginning of the following wall convergence on coarse particles. More details of the cyclical crushing process will be described in later sections. Essentially, with this work on Impulsive Segregation of a Bi-Disperse Mixture Between Outwardly Moving Walls, we seek an understanding of the part of the cyclic crushing process where one wall is moving away from the other to release the compacted particle bed mixture. The crushed material is then fluidized, and it is intended that fine material be preferentially swept away at that time.

In the following sections, brief descriptions of comminution methods are given, and then the cyclical comminution machine concept is explained.

1.1 Overview of Comminution Processes

1.1.1 Primary Crushing

Primary crushing is the first round of crushing for reducing large sized materials. There are three types of primary crushing equipment, each with its own distinctive operating characteristics: Jaw crushers, Gyratory crushers and Impact crushers. Jaw crushers work by squeezing the rock between the fixed and the movable sides of a tapered cavity. Fig. 1-1 illustrates a jaw crusher. Variations of pitch and swing have been tried, but most machines have a crushing angle of about 27 degrees between swing and stationary jaws. The dry finer material is discharged by way of gravity, and may go through a series of screens.

In gyratory crushers, fig. 1-2 for example, a cone is mounted on the upper end of a vertical shaft and the top of the shaft is held stationary while the lower end is rotated concentrically. If the cone is enclosed in a suitable housing, it will swing toward and away from the housing walls as it rotates. Anything caught between the cone and the housing walls will be crushed. The dry finer material is discharged by way of gravity. Gyratory crushers have the advantages of: (1) increased efficiency developed by the continuous crushing action and curved crushing faces, (2) the largest unrestricted feed

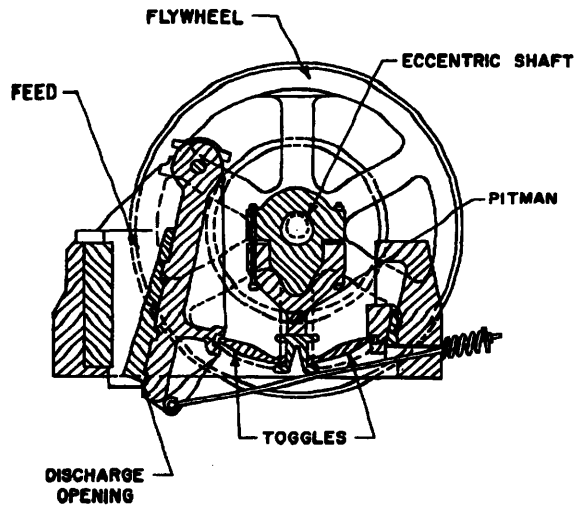


Figure 1-1: Jaw Crusher (picture scanned from Cummins & Given, 1973).

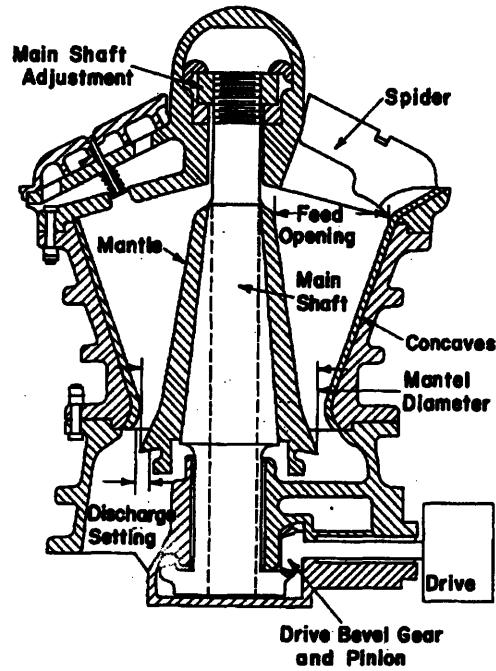


Figure 1-2: Gyratory Crusher (picture scanned from Cummins & Given, 1973).

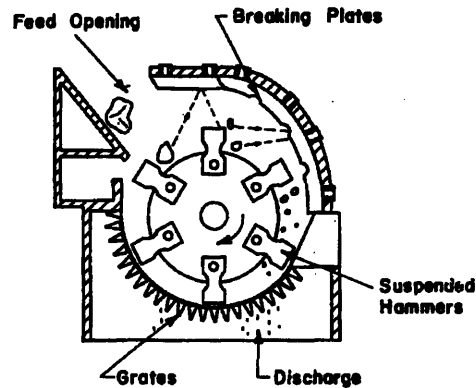


Figure 1-3: Impact Crusher: Hammer Mill (picture scanned from Cummins & Given, 1973).

opening available in comparison to other crusher types, and (3) a high range of sizes and capacities where rates of between 600 and 6000 tons per hour are required.

The converging-diverging wall motion of both jaw crushers and gyratory crushers is identical to that studied here, but the material transport mechanism (gravity) in both is quite different.

In impact crushing, material is reduced primarily through impact of the material with fixed or free-swinging hammers revolving with a central rotor. An impact crusher is shown in fig. 1-3. Benefits in using impact-type crushers are lower installed capital costs per ton of capacity, much greater capacity weight for weight of comparable Jaw and Gyratory crushers thus reducing installation cost and raising the feasibility for mobile units, production of more cubical product and generally, a finer product gradation. This may reduce the need for secondary crushing units. Impact crushers are not effective for strong materials.

1.1.2 Secondary, Tertiary and Quaternary Crushing

The cone crusher is used as a secondary, tertiary and fourth stage crusher in hard rock applications specifically. The cone crusher, shown in fig. 1-4, is designed like the normal gyratory crusher, except in the bottom half. The head, or one of the confining elements of the crusher, travels through a much greater distance and gyrates much

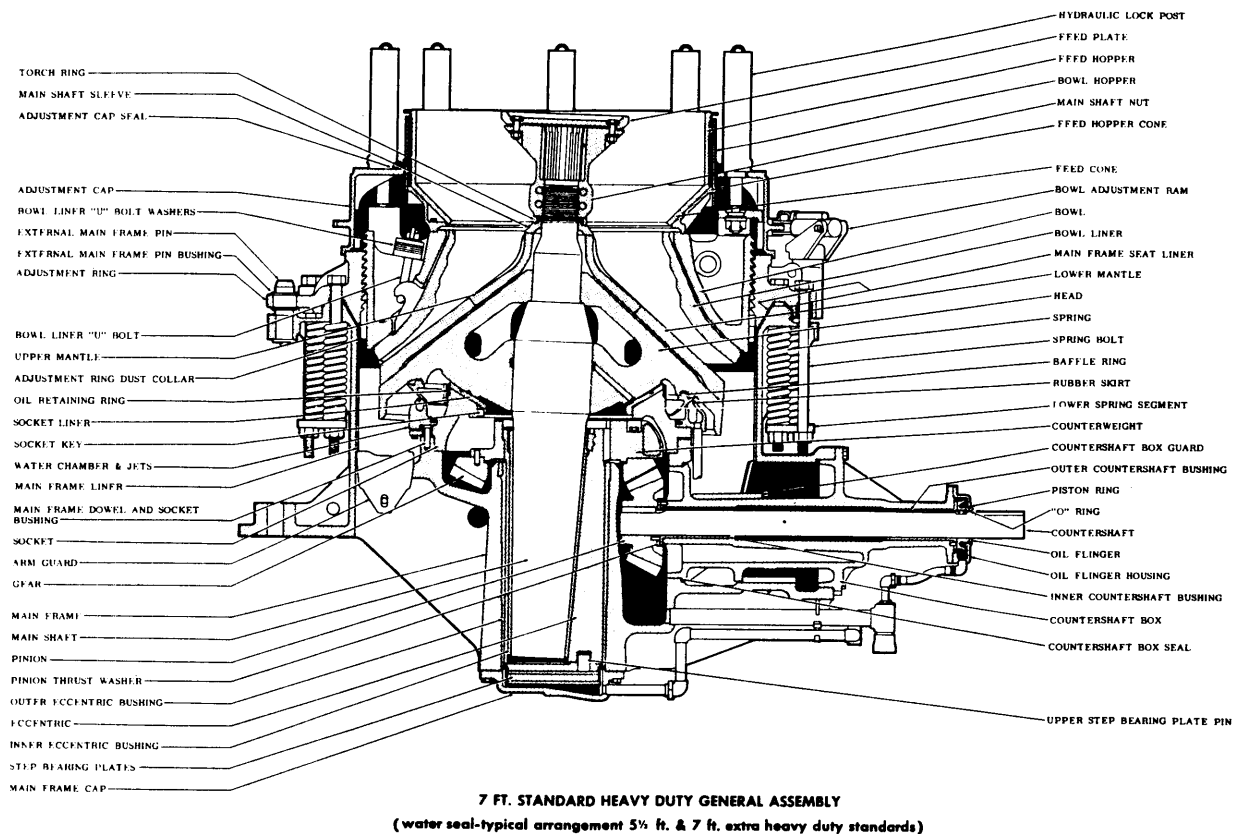


Figure 1-4: Cone Crusher (picture scanned from Mular & Bhappu, 1980).

faster in the cone crusher. The long movement changes the crushing stroke from pressure to impact, resulting in finer products than possible in a gyratory crusher. In tertiary crushing, a Short Head Cone crusher is commonly used. Maximum production is obtained when the crusher operates at or near full horsepower continuously. To achieve this, feed distribution and type of crushing cavity need to be considered. The feed material, made up of finer gradations interspersed within the coarse feed, is fed steadily, and in a controllable way. To meet variations in feed size and product requirements, the Short Head Cone is equipped with various designs of fine, medium, or coarse crushing cavities. Quaternary crushing is achieved through the Gyradisc, handling feed of less than 50 mm. Gyradisc crushers are different from conventional cone crushers in that comminution of material is achieved by a reduction process called Inter-Particle Comminution. This reduction process makes use of a combination of impact and attrition of a multilayered mass of particles.

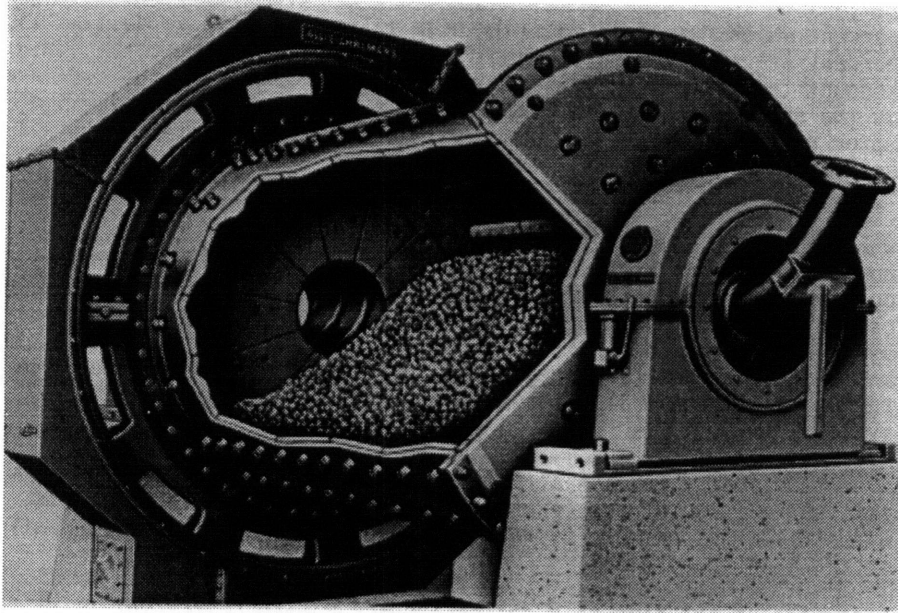


Figure 1-5: Ball Mill (picture scanned from Mular & Bhappu, 1980).

1.1.3 Fine Grinding

Grinding, the final stage of comminution, requires a large capital investment and frequently is the area of maximum usage of power and wear resistant materials. Grinding is most frequently done in rotating drums using loose grinding media which tumbles with the feed material as the drum rotates. Grinding media can be coarse pieces of the feed material itself, natural or manufactured non-metallic media, or manufactured metallic media such as steel balls. Fig. 1-5 illustrates a ball mill, which uses a manufactured metallic grinding material.

1.2 The New Design Concept

1.2.1 Material Transport

The ultimate goal of this comminution project is to create a more efficient machine design. One of the problems with present machines is that they do not adequately

accomplish material transport as an integral element of the comminution process. Proper material transport will remove the fine material left over after a crushing cycle. It would cause size-dependent segregation, so particles of various sizes may be placed in desired locations in the machine using variable fluid velocities, or swept out of the machinery entirely when adequately crushed. This would be a major advantage since choking problems can be avoided and large outputs can be obtained.

1.2.2 Proposed Machine Concept

A general cyclical comminution machine design, incorporating crushing and material transport working together in a cyclical process has been conceived. It is shown schematically in fig. 1-6. For simplicity, a cylindrical geometry is illustrated. The vertical section view has an inner member, positioned within a fixed external shell, and mounted on a drive shaft rotating eccentrically. Working fluid (generally water) flows vertically from the bottom of the machine. New coarse material is fed from the bottom and the fine (crushed) material is washed out the top of the machine. The gap, or flow cross-sectional area, is circumferentially changing because of the eccentric rotation of the drive shaft. This is seen in the two drawings in the right half of fig. 1-6 which represent unwrapped top and side circumferential views of the device. They show the idealized progression of the mixture of particles in a given cycle. In the side view, the left-most point on the figure is where crushing has just occurred and a mixture of coarse and fine material is fully compressed. In the region following, the walls have moved apart and particles are fluidized and segregated according to size by way of the upward flow. The fine material separates from the mixture by being swept upwards more rapidly by the fluid, and the cleaned coarse particles stay at the bottom, ready to be crushed again. For clarity, introduction of new coarse from the bottom is not shown in this figure.

Crushing is achieved in a region called the crushing zone where the gap diminishes. This is where the coarse material is crushed into a mixture, or rubble, of particles of various sizes. The top unwrapped view illustrates the path of the cylinder in a cycle and the corresponding varying gap thickness. These figures are a helpful,

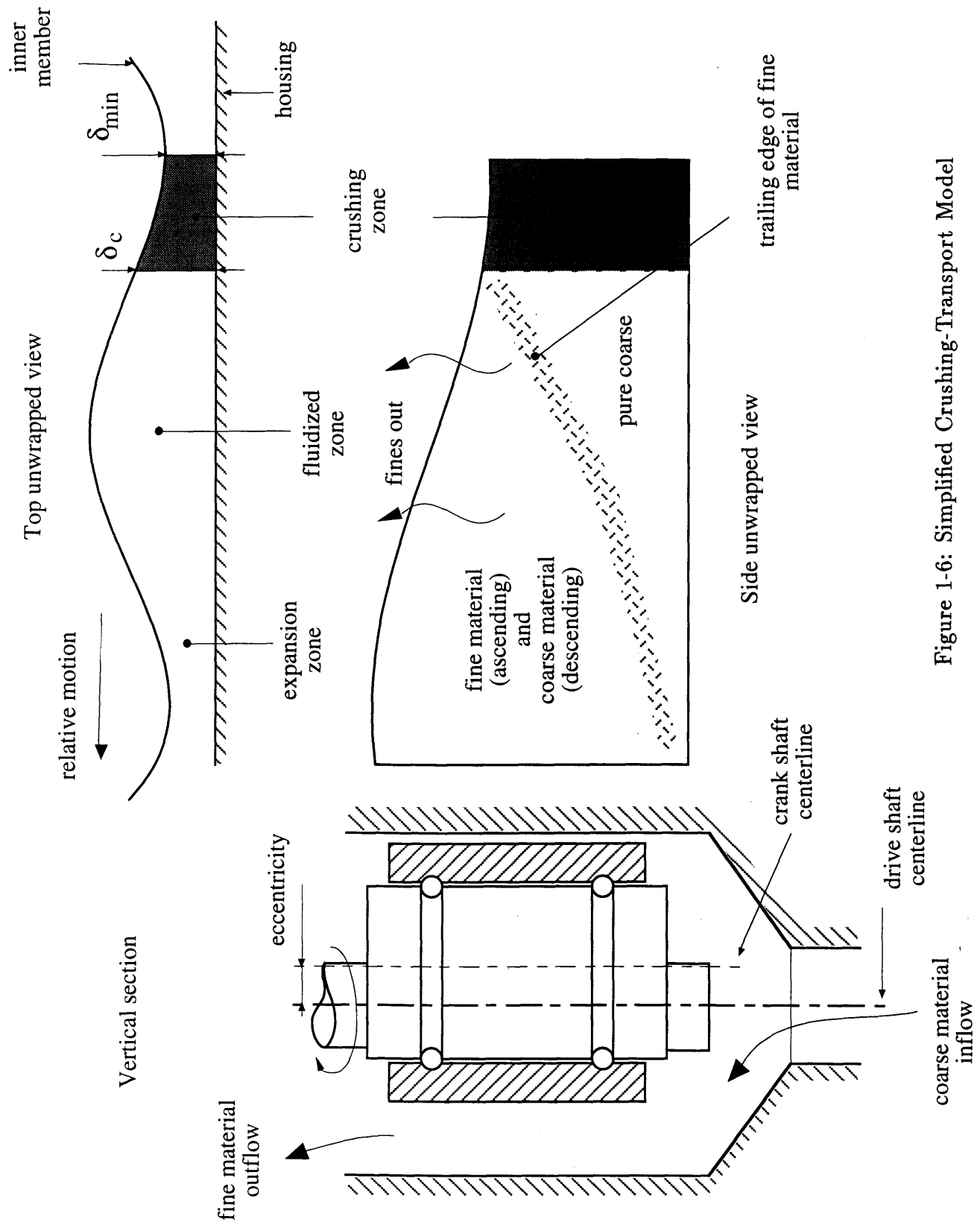


Figure 1-6: Simplified Crushing-Transport Model

yet a somewhat unrealistic simplification of the phenomena involved. Only one-dimensional bed behavior is considered here, while it is certain that secondary flows and recirculation regimes will play an important part. The behavior of the distinct sweeping out of the trailing edge of fine particles is probably unrealistic, especially when considering the three-dimensional system with irregular flow distribution and the volume change created by moving the wall out. Despite these simplifications, it is very useful in defining the problem and setting goals for design research.

In fig. 1-6, the ratio of minimum gap thickness, δ_{min} , to the gap spacing where particles are being trapped between two walls, δ_c , is drawn as

$$\frac{\delta_{min}}{\delta_c} = 0.78 \quad (1.1)$$

This particular value is based on bed fracture tests (Ghaddar, 1991, Misra, 1991), explained later in more detail, where this value corresponds to the bed compression (22%) for the maximum comminution efficiency.

An alternative to the cylindrical design in fig. 1-6 is shown in fig. 1-7, a conical crushing geometry. The inner conical member oscillates vertically, or more likely nutates, to provide the converging-diverging crushing action in the gap. The geometry of the device is such that fluid velocity decreases in the upward direction even though the gap between opposite walls is decreasing in that direction. Smaller particles move to the upper portion of the flow region, and larger remain in the lower. The intent is to create a distributed segregation, with particles moving upward successively as they are gradually reduced in size. This would make for energy efficient crushing, but is not clear that the non-vertical crushing chamber will permit fluidized segregation.

1.3 Previous Work in Comminution Program: Particle Fracture in Beds

Previous work in the comminution program (Ghaddar, 1991, Misra, 1991, Pflueger, 1988, Laffey, 1987, Larson, 1986, Easter, 1989) have explored fracture processes in

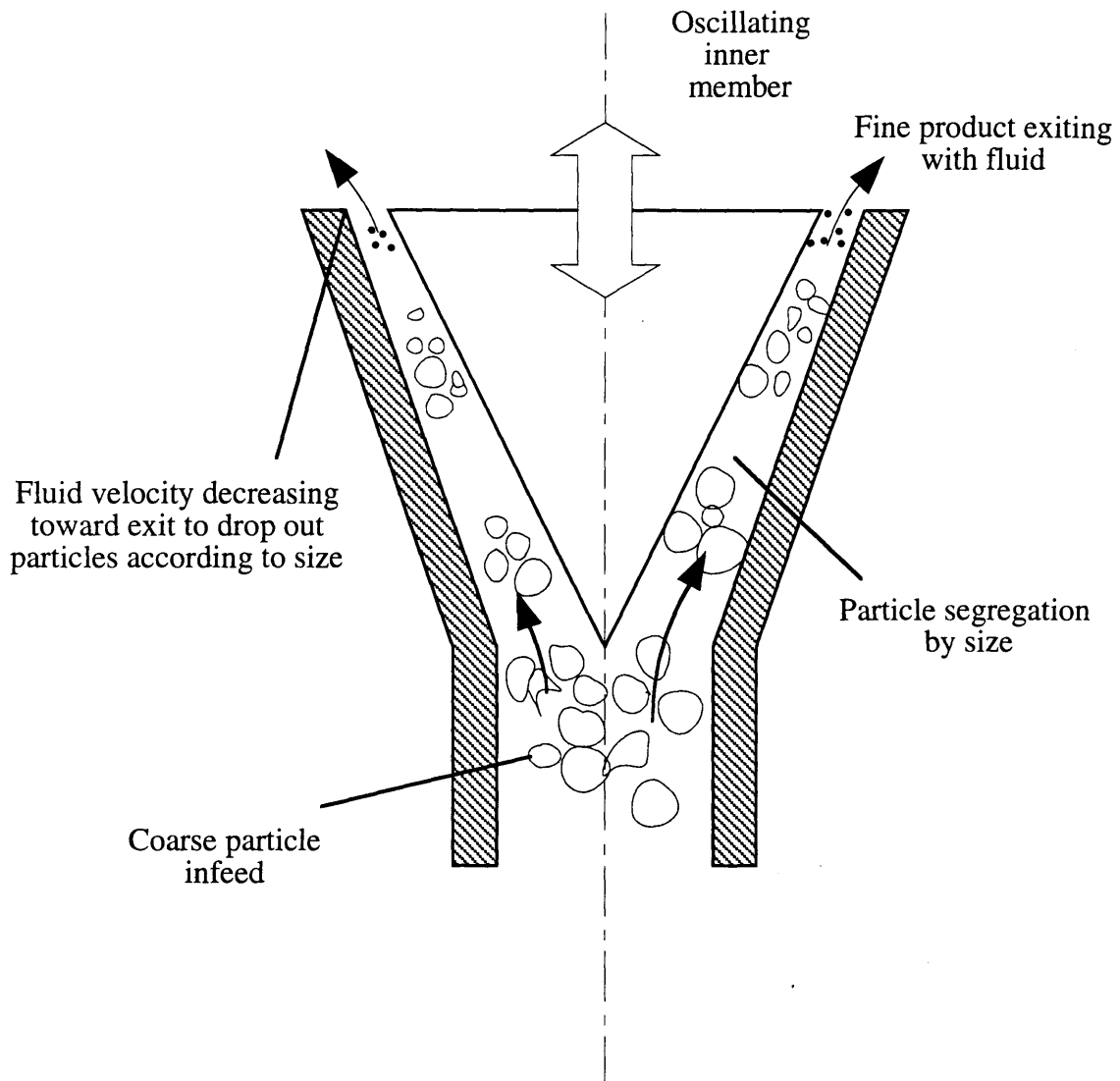


Figure 1-7: Conical Crushing Geometry

comminution through theoretical and empirical studies, as well as computer simulations. The goal of the work has been to determine the loading and bed conditions under which the efficiency of breakage of particles within the bed is maximized.

Throughout the breakage tests, spherical glass particles were used. It is easiest to identify breakage with this shape of particle and they are readily available. Ghaddar (1991) defined a simple but useful measure of “bed efficiency” within a particle bed and tested it on beds undergoing quasi-static compression. This definition is:

$$\text{bed efficiency} = \frac{\text{Energy required to fracture a particle in two point loading}}{\text{Energy required to fracture a particle within bed}} \quad (1.2)$$

This accounts only for the initial breakage of a particle within the bed and does not give credit for subsequent breakage of the fragments thus formed. However, these are the dominant occurrences within the bed up to the maximum efficiency compression. Ghaddar and Misra were able to relate the bed efficiency to some machine design parameters. For example, this bed efficiency definition can be used to determine the optimal conditions of bed compression and initial bed height.

Ghaddar presented Bed Efficiency as a function of compression, fig. 1-8, illustrating that optimal efficiency is obtained when the bed is compressed to 0.78 times the initial thickness (a load compression of 22%).

Fig. 1-9, shows a stress-strain curve for a 1-inch bed undergoing a quasi-static compression. It indicates three stages of compression. In the first stage, a gradual increase up to about 4% compression, energy is dissipated in overcoming the frictional forces due to the reconfiguration and repacking of the bed but little breakage occurs, and comminution efficiency is low. After about 4% compression, the stress remains about constant with increasing strain, as appreciable breakage occurs. The stress fluctuations are due to build up and subsequent destruction of frictional internal bed structures as fractures progress. In the last portion of the stress-strain curve, beyond 22% compression, the stress starts to rise again steeply as the available space between coarse particles is filled by fine material. Fracture is still taking place in this region,

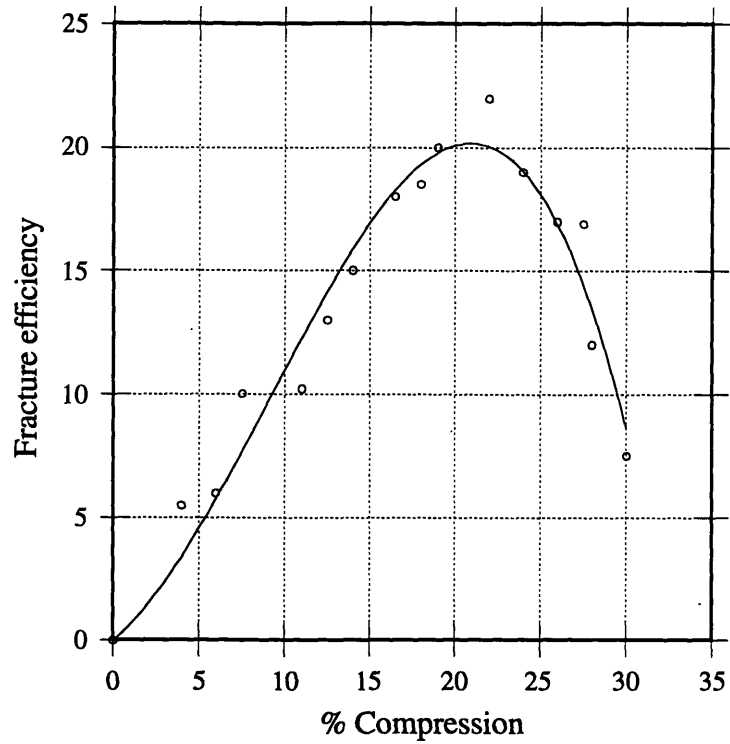


Figure 1-8: Fracture efficiency as a function of compression for 1 inch bed.

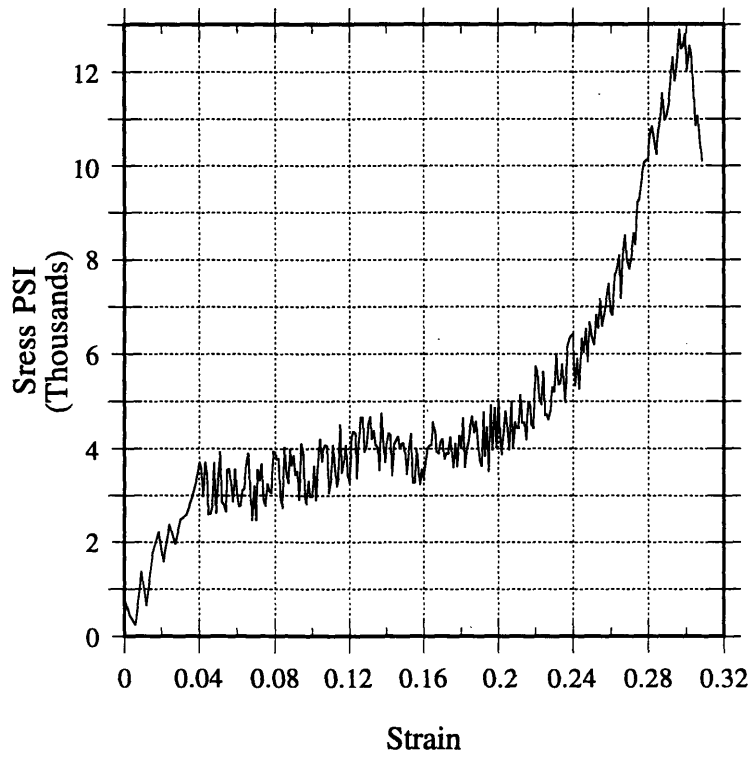


Figure 1-9: Typical stress-strain curve for 1 inch bed (30% compression).

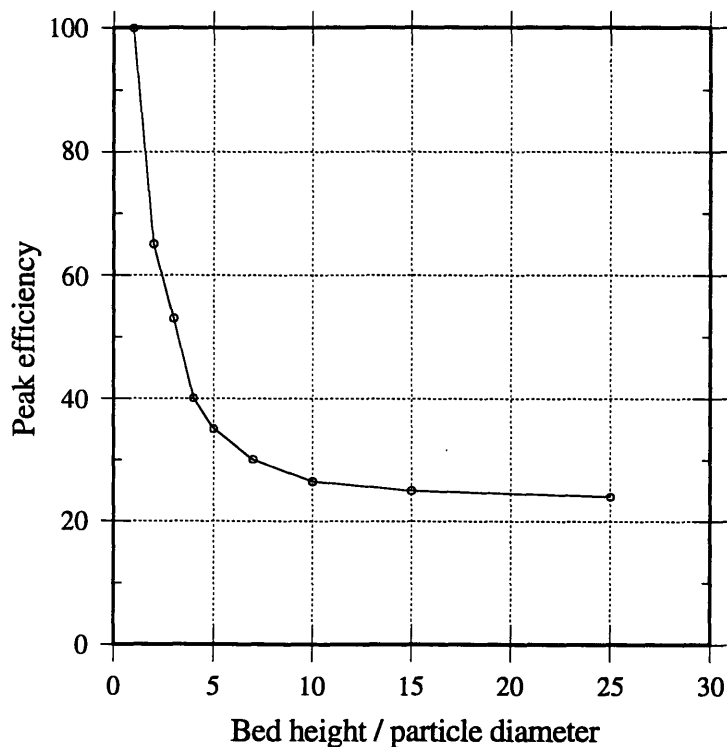


Figure 1-10: Peak fracture efficiency as a function of compression for 1 inch bed.

but the work done on the bed is increasing significantly compared to the work done during the middle stage. This low efficiency portion can be avoided by timely removal of fine material.

Fig. 1-10 is a curve of Peak Fracture Efficiency as a function of dimensionless bed heights from Misra. Bed efficiency is, by definition, unity for a monolayer of particles as, under this condition the particles are crushed individually between flat plates. Bed efficiency decreases rapidly for increasing bed heights within 5 particle diameters. It then levels off to a nearly constant value at a bed height of about 10 particles (the slow decline thereafter is believed to be a wall effect). Excellent bed efficiencies can be obtained using a gap of only a few particle diameters, but this comes at the expense of a very limited production rate. However, fig 1-10 suggests that a high production rate can be achieved at little additional cost in energy efficiency for bed heights beyond about 10 particle diameters.

1.4 Previous Work in Comminution Program: Particle Fluidization/Segregation

The present work describes impulsive segregation of a bi-disperse particle bed between outwardly moving walls, corresponding to the diverging wall portion of a crushing cycle. Previous work in the study of particle fluidization and segregation has focused on a fundamental understanding of transport and removal within the simpler configuration of stationary channel walls (Schiaffino, 1993). Specifically, it investigated two things: (1) Steady fluidization of fine particles within a fixed bed of coarse particles, and (2) Impulsive fluidization of a uniformly mixed bi-disperse particle bed.

1.4.1 Steady Fluidization of Fine Particles Within a Coarse Matrix

In (1), steady fluidization of fine particles in a fixed bed of coarse particles, the hindering effects of a fixed matrix of coarse particles on the fluidization of fine particles are studied, with the results compared with existing correlations for fluidization of mono-disperse spheres in vertical channels (Richardson and Zaki, 1954). A new correlation is proposed, in the form of the Richardson and Zaki correlation, but the containing channel dimension is replaced by the effective diameter of the coarse pore space, and one of the empirical coefficients is modified to obtain a better fit.

From theoretical arguments and experimental results, Richardson and Zaki obtained a relation for the liquid superficial velocity j_l (the volumetric flow divided by the total cross sectional area: $j_l = Q_l/A$) in terms of the particle volume concentration ν and two correlating parameters:

$$\log j_l = n \log(1 - \nu) + \log U_i \quad (1.3)$$

Here, n is the slope of the log-log curve and $\log U_i$ is the intercept on the $\log j_l$ -axis at $\nu = 0$. Also, with the help of dimensional analysis, Richardson and Zaki correlated the coefficient n with the ratio between the particle diameter, d , and the pipe diameter,

D , and with the Reynolds number, Re_∞ , based on the settling velocity U_∞ of an individual particle in an infinite stationary liquid. Reynolds number is given by

$$Re_\infty = \frac{\rho_l U_\infty d}{\mu_l} \quad (1.4)$$

where ρ_l and μ_l are fluid density and viscosity, respectively. The Richardson and Zaki correlation for n for the $1 < Re_\infty < 10$ range of interest to the present study was:

$$n = (4.45 + 18d/D)Re_\infty^{-0.1} \quad (1.5)$$

Richardson and Zaki also compared the values of U_i with those for the terminal velocity, U_∞ , and they arrived at the following empirical correlation:

$$\log U_\infty = \log U_i + d/D \quad (1.6)$$

The difference between U_∞ and U_i is attributed to the velocity gradient created near the wall.

For fluidization of fine particles through the test section full of coarse particles, Schiaffino defined the liquid superficial velocity and the fine particle concentration ν with respect to the interstitial space of the coarse medium as

$$j_l = \frac{Q_l}{A(1 - \nu_c)} \quad (1.7)$$

$$\nu = \frac{V_f}{V - V_c} \quad (1.8)$$

Above, ν_c is the coarse particle concentration, typically 55% for a packed bed. The total volume of coarse and fine particles (V_c and V_f) are known as the experimental configuration is established. The instantaneous value of the relevant experimental volume, V , is obtained by visually measuring the height of the fluidized fines in the coarse matrix and knowing the test section cross sectional area. (The test section volume occupied by the coarse matrix does not change as the coarse material is not

fluidized). In Schiaffino's experimental work, a plexiglass test section of rectangular cross section of 10 mm X 35 mm and height of 200 mm was used, and glass particles of diameters of 0.15, 0.2, 0.3 and 0.4 mm for the fine particles, and 2, 3 and 4 mm for the coarse particles were used. This work produced the bi-disperse curves of figs 1-11, 1-12, 1-13 and 1-14. These are described by the above specialized equations, (1.7) and (1.8). Since they lie on straight lines, as is the case with a single species, an equation of the form of (1.3) would appear to be a good choice to correlate the results. However, since the slopes and intercepts of these lines depend significantly on the size of the fine and coarse particles, we see that the coarse medium has a large hindering effect on the fluidization of the fine particles. That is, the intercept, $\log U_i$, decreases while the slope of the lines increases, as the particle size ratio (d/d_c) increases. Schiaffino has summarized results for the equation in Table 1.1. In modifying the correlations of Richardson and Zaki for the case of fluidization of fine particles within a stationary coarse matrix, Schiaffino began by noting that the primary difference between the two situations is in the geometry of the fluidized region. Therefore, he could use the same approach for the two cases, provided that a different scaling parameter is used in place of the channel diameter, D , appearing in equations (1.5) and (1.6). The best new scaling parameter, which took into account the size of the passages formed by the coarse particle bed and their meandering shape, was the hydraulic diameter based on the volume and the wetted surface of the coarse pore region. Schiaffino proposed

$$D = \frac{4 \times \text{Coarse Pore Volume}}{\text{Wet Surface of Coarse Medium}} = \frac{2(1 - \nu_c)d_c}{3\nu_c} \quad (1.9)$$

Since ν_c , concentration of the coarse bed, was always close to 55%, D is about $0.545d_c$. Schiaffino determined that Richardson and Zaki's correlation (1.3) works well for this study of fluidized fines in a coarse matrix using not only the new hydraulic diameter, but also using a modified correlation for n :

$$n = (4.45 + 5.74d/D)Re_\infty^{-0.1} \quad (1.10)$$

The correlation for terminal velocity (1.6) remains unchanged.

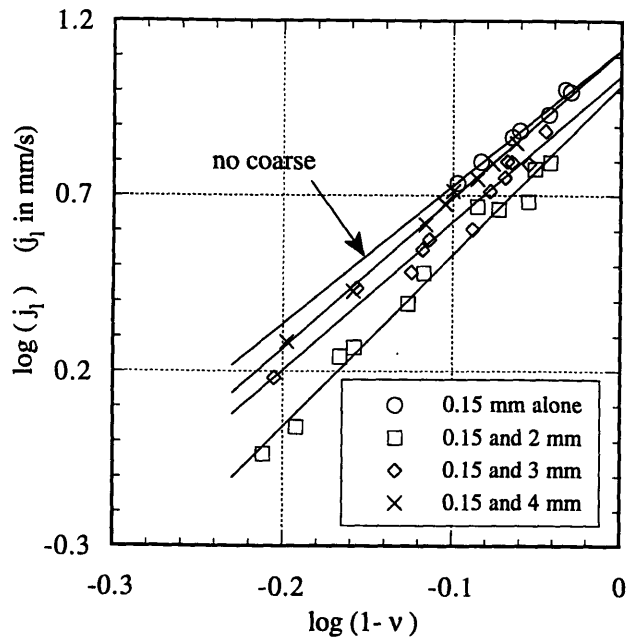


Figure 1-11: Experimental results for fluidization of 0.15 mm particles in a coarse bed.

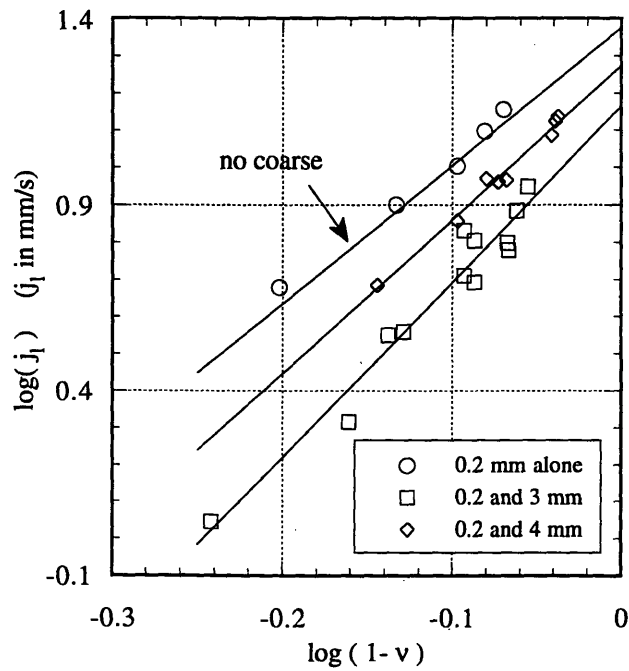


Figure 1-12: Experimental results for fluidization of 0.2 mm particles in a coarse bed.

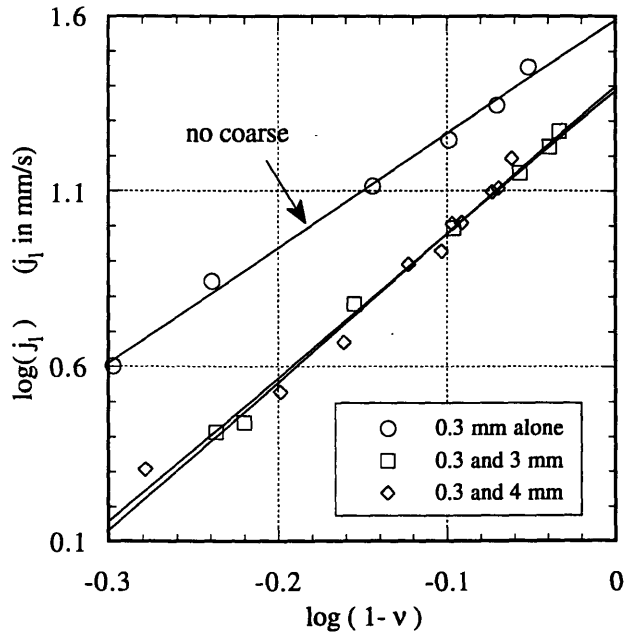


Figure 1-13: Experimental results for fluidization of 0.3 mm particles in a coarse bed.

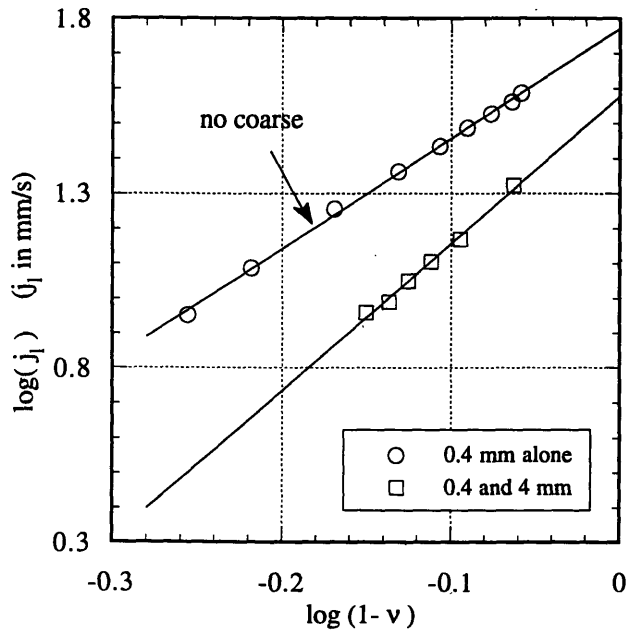


Figure 1-14: Experimental results for fluidization of 0.4 mm particles in a coarse bed.

d_c (coarse)	d (fines)	size ratio d/d_c	U_i	95% confidence limits		n	95% confidence limits		correl. coeff.
[mm]	[mm]		[mm/s]		[mm/s]				
-	0.40	-	59.09	+/-	1.76	3.15	+/-	0.09	0.999
4.00	0.40	0.100	37.94	+/-	4.12	4.22	+/-	0.38	0.996
-	0.30	-	39.04	+/-	4.66	3.27	+/-	0.28	0.997
3.00	0.30	0.100	25.25	+/-	1.84	4.23	+/-	0.21	0.998
4.00	0.30	0.075	24.45	+/-	3.19	4.10	+/-	0.38	0.990
-	0.20	-	23.71	+/-	3.93	3.50	+/-	0.53	0.994
3.00	0.20	0.067	14.58	+/-	2.72	4.72	+/-	0.63	0.974
4.00	0.20	0.050	18.73	+/-	1.51	4.13	+/-	0.42	0.992
-	0.15	-	13.18	+/-	0.69	3.92	+/-	0.35	0.995
2.00	0.15	0.075	10.41	+/-	1.28	4.87	+/-	0.39	0.992
3.00	0.15	0.050	11.08	+/-	1.21	4.20	+/-	0.41	0.986
4.00	0.15	0.038	13.14	+/-	0.72	4.26	+/-	0.19	0.998

Table 1.1: Least square fitting of fluidization experimental data in log-log representation (Figs. 1-11 to 1-14).

1.4.2 Impulsive Fluidization of a Bi-Disperse Mixture

Schiaffino also studied (2) impulsive fluidization of a uniformly mixed bi-disperse particle bed in a stationary wall channel. This was undertaken as the first step in examining the fundamental questions related to the removal of fine particles from the rubble of coarse and fine particles produced by a crushing cycle.

In these tests, the bi-disperse mixture held in a plexiglass test section is suddenly subjected to a constant upward liquid flow rate, or step flow, produced by a positive displacement pump. From Schiaffino's typical test sequence, fig. 1-15, it is possible to observe in detail the progressing segregation process. Here, frames are spaced 1/6th of a second apart. The sizes of the particles were 0.2 and 4.0 mm. After the step flow is introduced, the entire mixture moves upward as a solid plug, forming a void underneath the plug. As the plug continues to rise, coarse particles in the lower layers of the plug then begin to fall through the void because the liquid velocity is always less than the coarse particle fluidization velocity. Fine particles, however, are fluidized and swept upward within the void so that the effect can be seen as a sweeping upward of the fines and a dropping out of the coarse in a wave-like progression of the void. Schiaffino determined fine particle percolation through the compact coarse matrix is not dominant in the segregation process. The fines remain within the plug until exposed to the advancing void. As the advancing void approaches the top of the plug, when only a few coarse particle layers remain, the wave breaks through in an unstable manner, momentarily propelling the final coarse particle layers upward into the upper test section. The final result is an accumulation of cleared coarse particles at the bottom of the test section while the fines remain fluidized above the coarse. The range of flow rate must be high enough to form the void and fluidize the fines, but low enough so the coarse are not fluidized.

Schiaffino performed a number of tests for different conditions. He used fine particles in sizes of 0.2 and 0.4 mm diameter, and coarse particles of 2, 3 and 4 mm. He also used three test sections with different aspect ratios. These test conditions are summarized in Table 1.2, and the geometrical characteristics of the three test sections are summarized in Table 1.3. Three test sections were used, having cross sectional

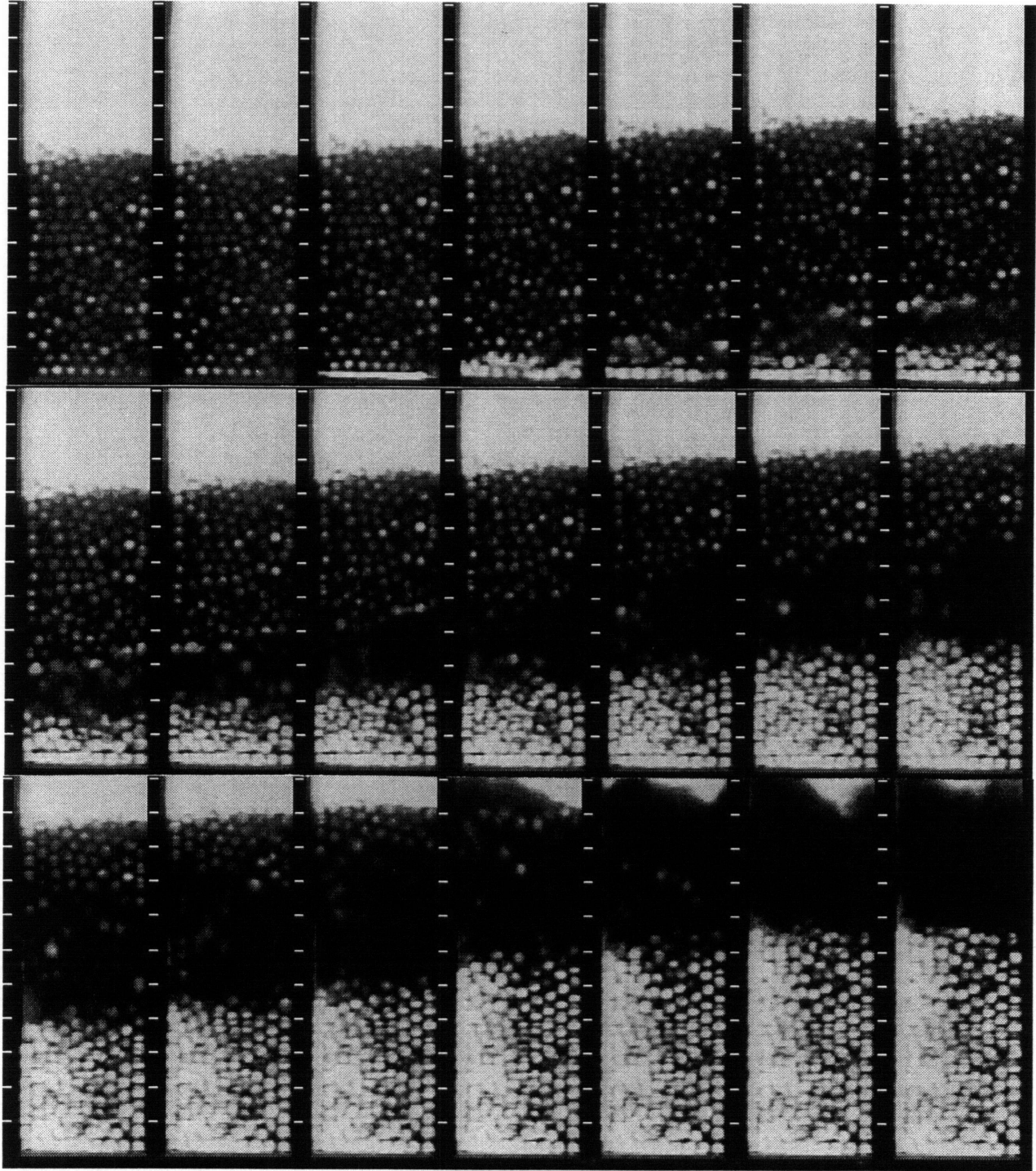


Figure 1-15: Sequence of video images spaced 1/6th of a second of an impulsively fluidized mixture of 0.2 mm fine and 4.0 mm coarse particles.

d_c [mm]	d_f [mm]	size ratio	J_1 [mm/s]	h_o/d_c	TS
2	0.2	0.1	3-90	15-35	TS1
3	0.2	0.07	3-25	10-22	
4	0.2	0.05	3-25	9-17	
2	0.4	0.2	15-90	18-22	
4	0.4	0.1	15-90	10-18	
2	0.4	0.1	8-40	18-28	TS2
4	0.4	0.05	8-40	15	
4	0.2	0.05	9-40	10-20	TS3

Table 1.2: Summary of test conditions for impulsive fluidization tests.

Name	Width [mm]	Depth [mm]	Hydraulic Diameter [mm]
TS1	35	10	15.6
TS2	70	10	17.5
TS3	28	28	26.4

Table 1.3: Geometrical dimensions of the three test sections used for impulsive fluidization.

dimensions of 35 mm X 10 mm (TS1), 70 mm X 10 mm (TS2), and 25 mm X 28 mm (TS3). These were chosen in relation to the size of the coarse particles used (2 - 4 mm) to have ratios of gap width to sphere diameter of 2.5 to 5. These correspond to bed dimensions of high crushing efficiency. The thinking behind the creation of the test sections is that in TS1 and TS2, the aspect ratio is changed in doubling the width. TS3 has the same cross-sectional area of TS2 and therefore the same fluid velocities, but has a higher hydraulic diameter with depth increased to 25 mm. As in the steady fluidization tests, the coarse bed packs to a volume concentration of 55%. The fines fill the pore space in the coarse medium, and have concentrations of 57 - 58%.

Schiaffino used video image analysis techniques to quantify the events of his tests. Shown in fig. 1-16 is a sample of the measurements he made. The initial height of the bed is h_o . The speed of the upward moving top interface is U_t . The speed of the lower interface associated with the depletion of the plug is U_b . The depletion velocity of the rising plug, U_{dep} , is defined as:

$$U_{dep} = U_b - U_t \quad (1.11)$$

The critical time, t_{cr} , is the time interval from initiation of the flow to break through at the top of the plug. The final item Schiaffino measured was the fraction of fine particles removed from the mixture. He did this by backlighting the test section and relating luminance values of a region to the fine suspension concentration. The lower the luminance of the region, the higher the fines concentration value, as quantified in empirical calibration tests.

Schiaffino had many interesting results, the first of which is seen in fig. 1-17. It is upward bed velocity, U_t , at given liquid superficial velocities for the large variety of test conditions (Table 1.2). With increasing liquid superficial velocities, the plug of particles lifts faster as one would expect, but the slip, or difference between fluid velocity and fine particle velocity, also increases. Schiaffino notes that upward bed velocity, U_t , does not show any clear dependence on the particle size and test sec-

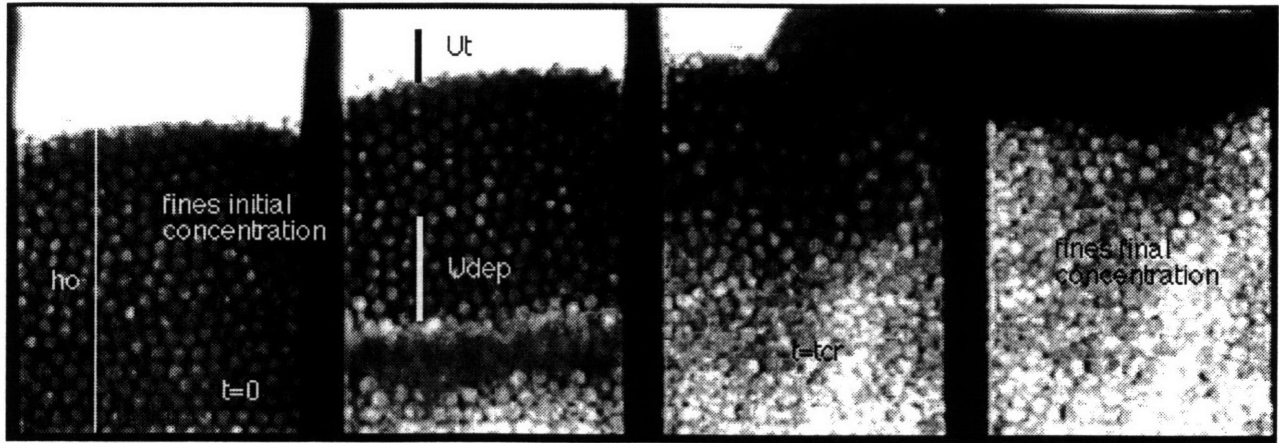


Figure 1-16: Measured quantities in impulsive fluidization tests.

tion dimensions. Next, Schiaffino looked at depletion velocity, U_{dep} , as a function of superficial liquid velocity, j_l , shown in fig. 1-18. It is important because it controls the time required to achieve final segregation (t_{cr}) for a given bed height. Note that depletion velocity does not seem strongly affected by the size of the particles, and is nearly constant over the range of conditions investigated with a small increase at the higher flow rates. Also, since tests run in differing containing geometries differed very little in depletion velocity, the depletion velocity is more a function of the particle raining mechanism than of the confining geometry. Beyond these basic results, Schiaffino addressed design-related questions by looking at segregation speed, segregation process critical height, and fines removal fraction, all important criteria for building a crushing device.

Segregation speed is important in that it indicates how long the crushing machine cycle must last. A fast segregation speed means that the machine cycle can be run at a high frequency and thus process a high through flow. Schiaffino shows results on segregation speed in fig. 1-19 as the ratio of initial bed height (h_0) to critical breakage time (t_{cr}) plotted against j_l . The segregation speed increases at a small slope as fluid flow is increased, showing a faster removal process is obtained at high liquid velocities. This is related to the increasing depletion velocity at higher flow rates (Fig. 1-18). Also, it is related to the increasing slip between plug and liquid at higher j_l values (Fig. 1-17) which implies a higher relative flow rate through the plug and a tendency

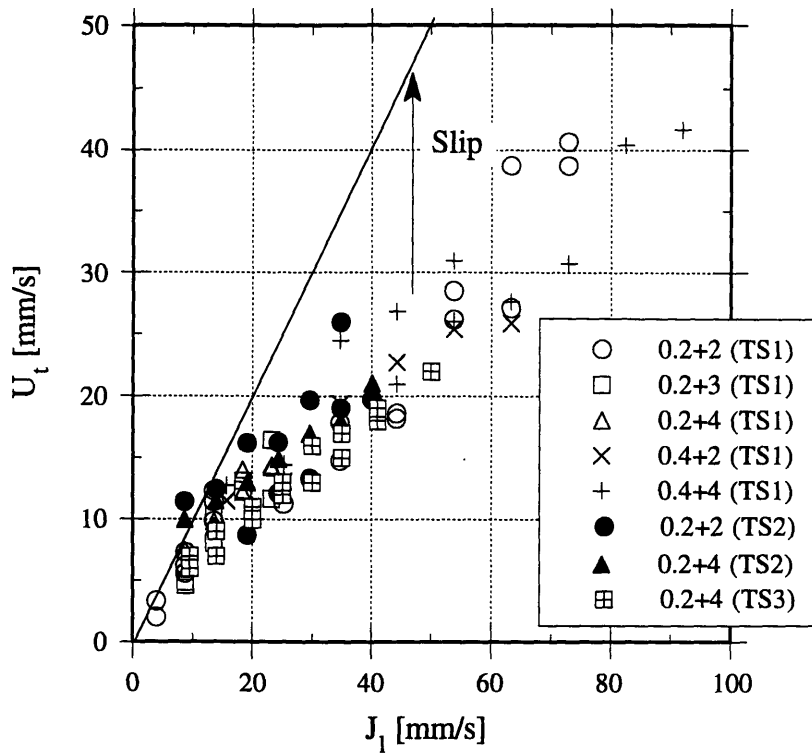


Figure 1-17: Upward Bed Velocity.

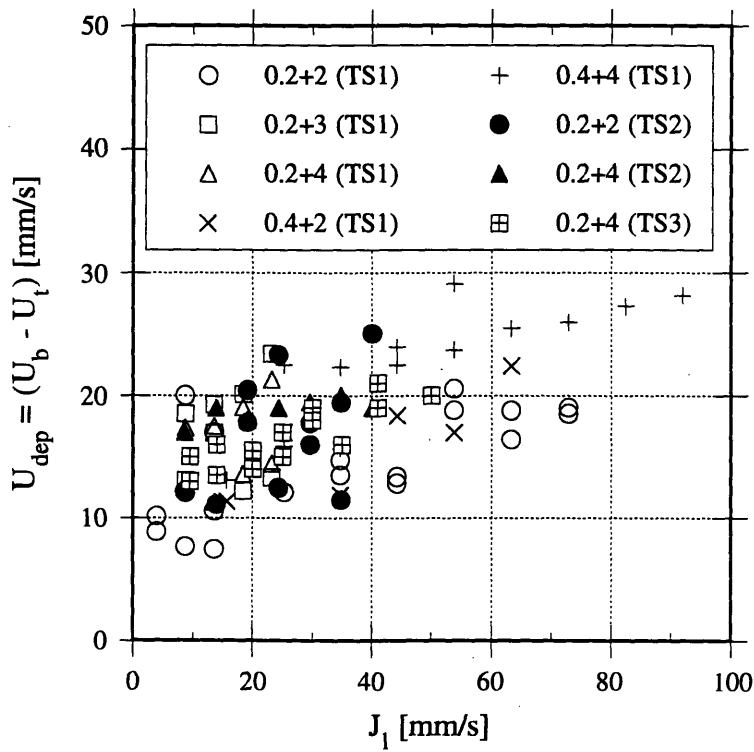


Figure 1-18: Depletion Velocity of the rising plug, as measured by an observer moving with the same velocity of the plug (U_t).

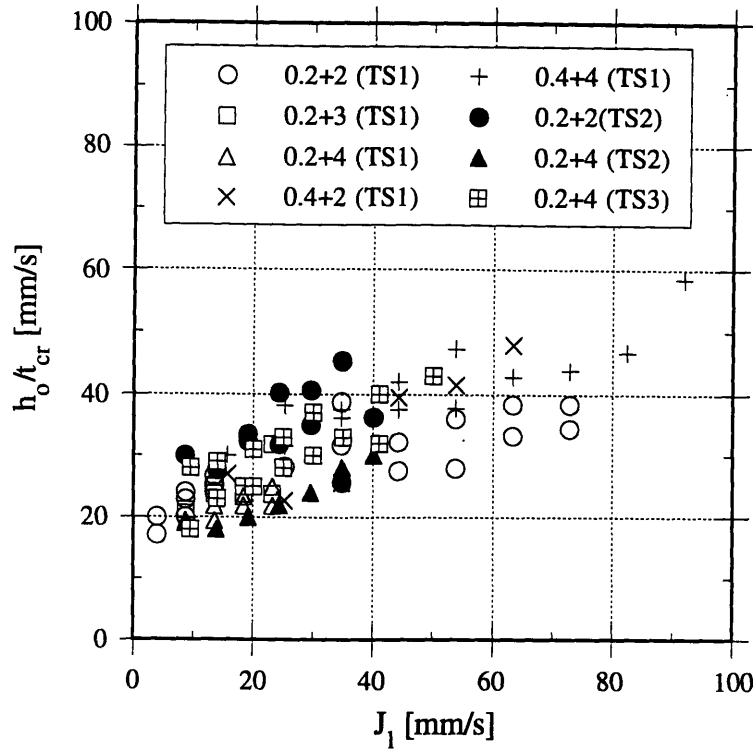


Figure 1-19: Segregation speed.

to break through more easily because of the higher force of the fluid on the particles. Schiaffino also determined a critical height, h_{cr} , at which an instability occurs and the fluid breaks through the rising plug. He took h_{cr} through the following indirect measurement:

$$h_{cr} = h_o - U_{dep} t_{cr} \quad (1.12)$$

Shown in fig. 1-20 is non-dimensionalized critical height versus j_l . The plot is designed to show a fingering phenomena occurring in the taller beds. That is, while the wave front progresses upward in the taller beds, it is more likely to develop local instabilities which create arching or fingering of the lower plug interface. In many instances, the lower plug interface starts relatively flat and then progresses according to irregular or fingered patterns. This creates the conditions for the void region to reach the top layers and to break the plug faster than it would with a flat interface. The critical height values for taller beds are consistently greater than those for shorter beds.

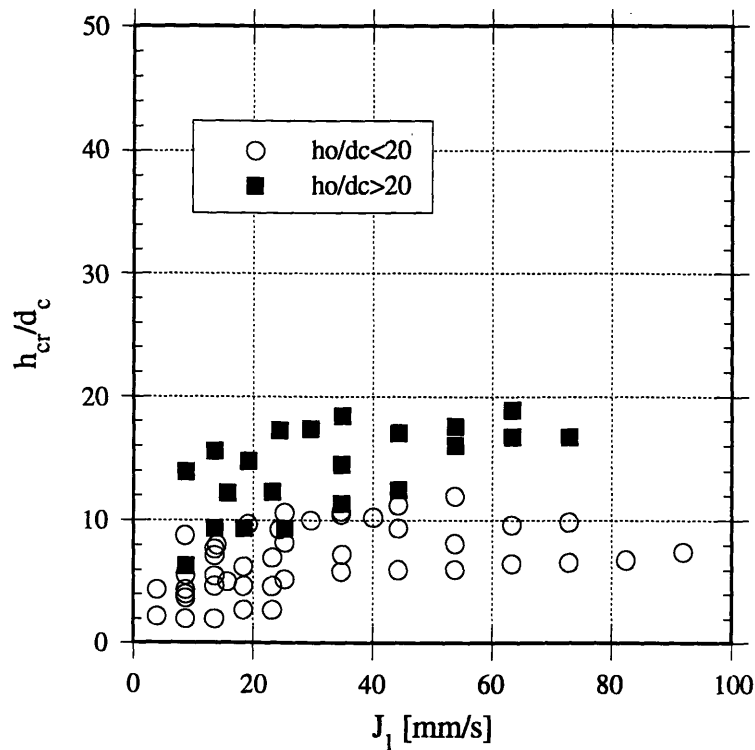


Figure 1-20: Non-dimensional critical height. Data are grouped according to non-dimensional initial bed height.

Fines removal fraction of the segregation process is shown in fig. 1-21. For superficial fluid velocities greater than the fine particle terminal velocity (22 mm/s for the 0.2 mm and 54 mm/s for the 0.4 mm), the coarse bed is almost completely cleared of fine particles, with a removal rate approaching 100%. This is because when the void forms and the coarse rain through it, the remaining fines do not easily settle under the superficial liquid velocity greater than their terminal velocity even when they are in a fairly concentrated condition. Those fines remain fluidized. For superficial liquid velocities less than fine terminal velocity, fines are partially carried downward within the falling coarse.

Schiaffino's experimental results prove to be useful, informative background for the following work in this paper. There will be similarities and references throughout this work.

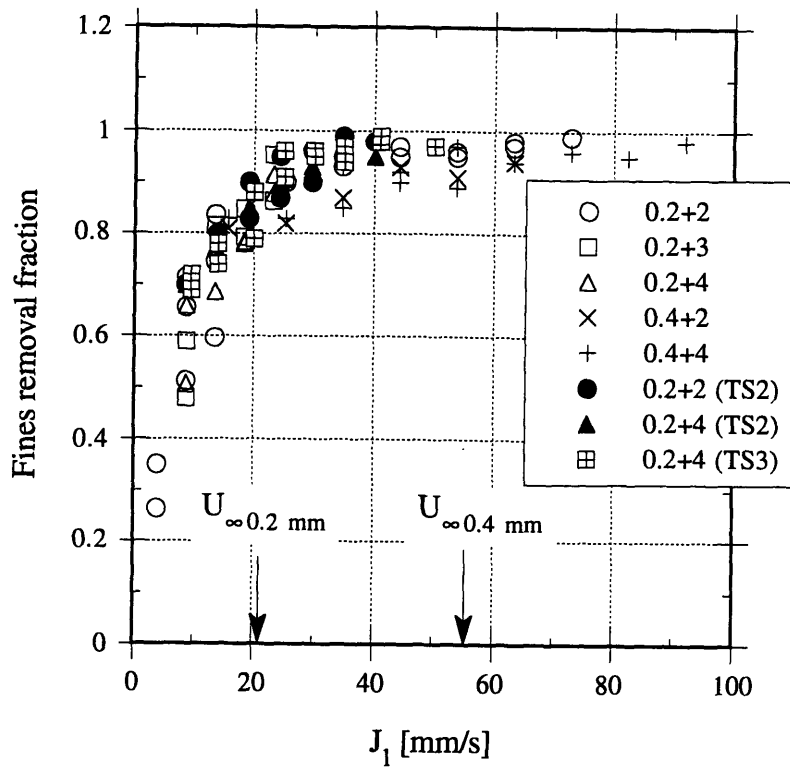


Figure 1-21: Fine particle removal.

Chapter 2

Impulsive Segregation of a Bi-Disperse Mixture Between Outwardly Moving Walls

2.1 Overview of Experimentation

This experimental investigation simulates the portion of the proposed crushing cycle in which the opposing walls are moving apart and the crushed material is fluidized. Although the test section does not simulate the “rolling” action of the inner member away from the outer member of the crusher nor the multi-directional flows in the actual crushing machine, its one-dimensional outward motion and one-directional upward flow do provide some insight into the behavior of the proposed design.

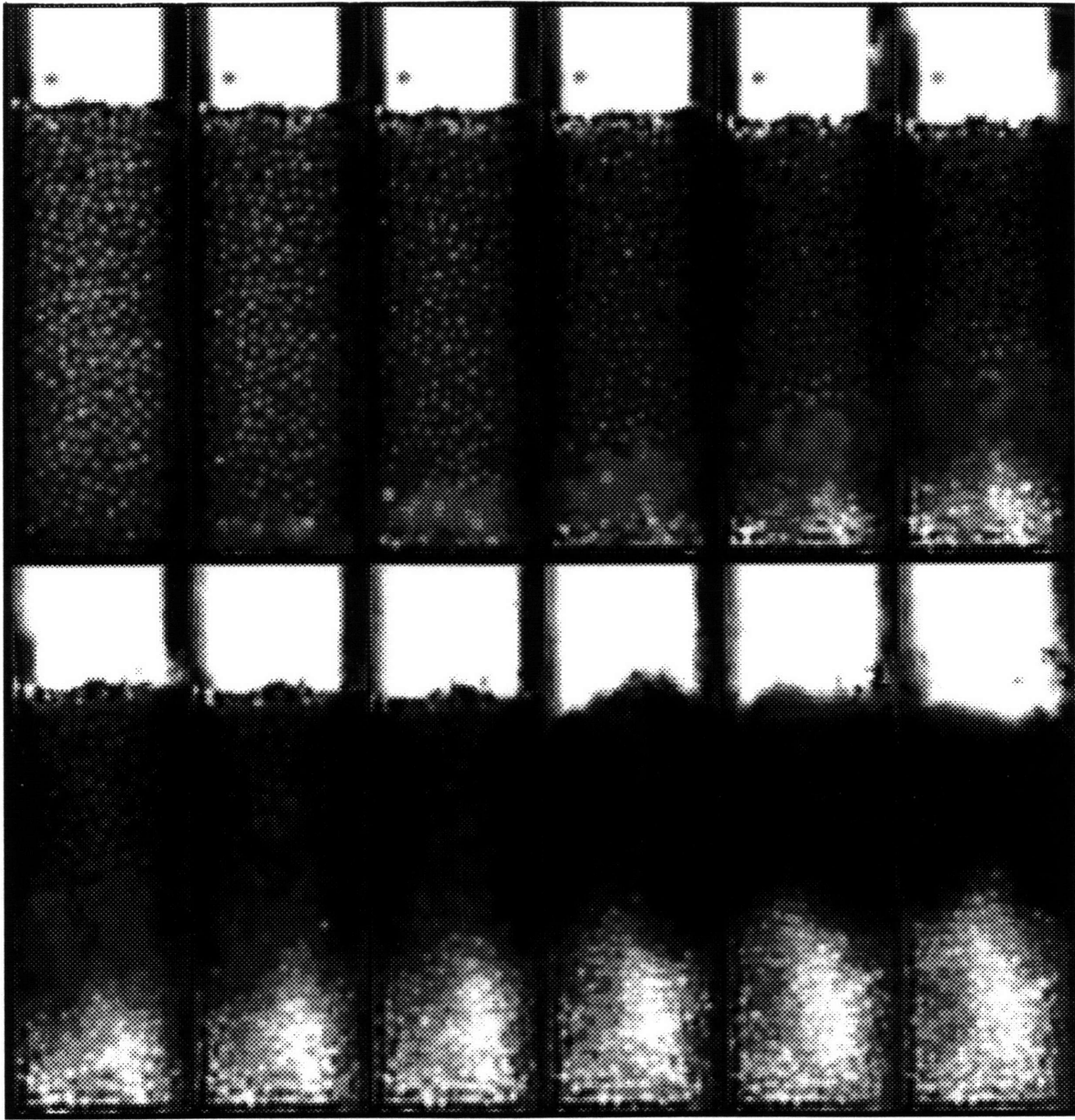
The experiments were performed in a vertical test section, containing a uniformly mixed bed of spherical glass particles of diameters 0.2 and 3.0 mm. This diameter ratio of 15:1 was convenient for setting up repeated tests because the fines freely filtered back into the coarse medium. The volume concentration of the coarse is on the order of 50-55%. The fines fill the void of the coarse medium, and their concentrations in the coarse pore space is in the range of 54-55%. Weights of fine and coarse particles were carefully measured so that the mixture in the test section was uniform and had a bed height of 98 mm. The total test section height available for expansion is 160

mm, because some extra height must be preserved for the upward expansion of the fluidized plug. The working liquid was water.

The test section containing the uniformly mixed bi-disperse mixture is simultaneously subject to an impulsively initiated constant volume flow rate from the positive displacement device and a constant outward wall velocity from a motor and pulley drive mechanism. The simultaneous start of the two events, flow and wall motion, is achieved through adjustment of a timing delay device which compensates for differing system time delays characteristic of the flow and of the wall motion drive systems.

2.1.1 Events Occuring in Time

To visualize the events that characterize these experimental tests, it is best to show a sequence of video images. Fig. 2-1 shows a sequence of video images spaced 1/6th of a second. The Inlet Flow Rate is $Q_{li} = 11,000 \text{ mm}^3/\text{s}$, corresponding to superficial velocities from 27.5 mm/s to 14.9 mm/s as the chamber width varies, and Wall Velocity is $V_w = 3.0 \text{ mm/s}$. In the range of experimental tests done (see section 2.5), this example is a low Inlet Flow Rate, and a low Wall Velocity. The fine particles are a mixture of black and white 0.2 mm glass spheres, and the coarse are 3 mm transparent glass spheres. The segregation process seen here is similar to that seen by Schiaffino in his impulsive fluidization in a constant container tests. The flow and the wall motion are initiated simultaneously. The mixture appears to be lifted as a plug with a void forming underneath. Lower layers of the plug precipitate through the void since the liquid velocity is smaller than the coarse particle fluidization velocity. Unlike the stationary wall tests, the top of the plug does not always rise in these tests. This is because of continuity. The outward moving wall, perpendicular to the snapshots, creates an increasing volume in the test section that the plug expands into. If the lateral expansion volume is greater than the upward motion at the bottom of the plug, the top of the plug may stand still or recede. Although a rising plug, as seen in Schiaffino's constant cross-sectional area tests, is not typical of these tests, other features are similar. For example, the upward motion of the plug is accompanied by the wave-like progression of a region where segregation



t_{cr}

t_{pr}

Figure 2-1: Sequence of Video Images (spaced 1/6th second). $Q_{li} = 11,000 \text{ mm}^3/\text{s}$, $V_w = 3.0 \text{ mm/s}$.

occurs between the coarse settling particles and the fine particles which are kept in suspension. Schiaffino noted that the formation of the void between the upward moving plug and the settled bed appears important for the segregation process. In this work, segregation is also enhanced to some extent by the outward motion of the movable wall which “opens” the plug to permit greater percolation of the fines through the coarse material. Particle percolation, however, is not dominant even with the outwardly moving wall. Essentially, at the velocities tested here, the fines remain within the plug until exposed to the wave-like pocket. The net result is the accumulation of a cleared coarse bed at the bottom of the test section, while the plug is shrinking in height. When the depletion of the plug is such that only a few particle layers are left, the remaining coarse material breaks suddenly in an unstable manner at a time Schiaffino called critical time, t_{cr} , or time of plug breakage. After the critical time, the remaining coarse particles settle in the midst of a cloud of the fines pushing upward. This is because liquid flow rates in these tests are always higher than the terminal velocity of the fines, but lower than that of the settling coarse. The instant of time when the final coarse particles from the plug settle to the pile of coarse on the bottom is called the process time, t_{pr} . After process time, the final condition is of the fines fluidized on top of the stationary, cleared coarse bed. All of this is seen in fig. 2-1, a typical sequence of video images of the experimental test. The sequence of events in a typical test is shown in fig. 2-2 in a different form. This shows the behavior of the interfaces in the mechanical fluidized segregation process, and the critical time, t_{cr} , and process time, t_{pr} . Process time, t_{pr} , relates to the design concept as the length of time necessary to achieve complete segregation of coarse and fine materials (in a bi-disperse mixture of spherical particles).

2.1.2 Measured Results

In order to answer design questions, and to examine a range of physical phenomenon, three separate measures of the fluidized mechanical segregation process were defined. They are (1) a Clearing Speed, or how quickly the segregation process occurs, defined as final bed height divided by process time, h_f/t_{pr} (2) Fines Removal Fraction,

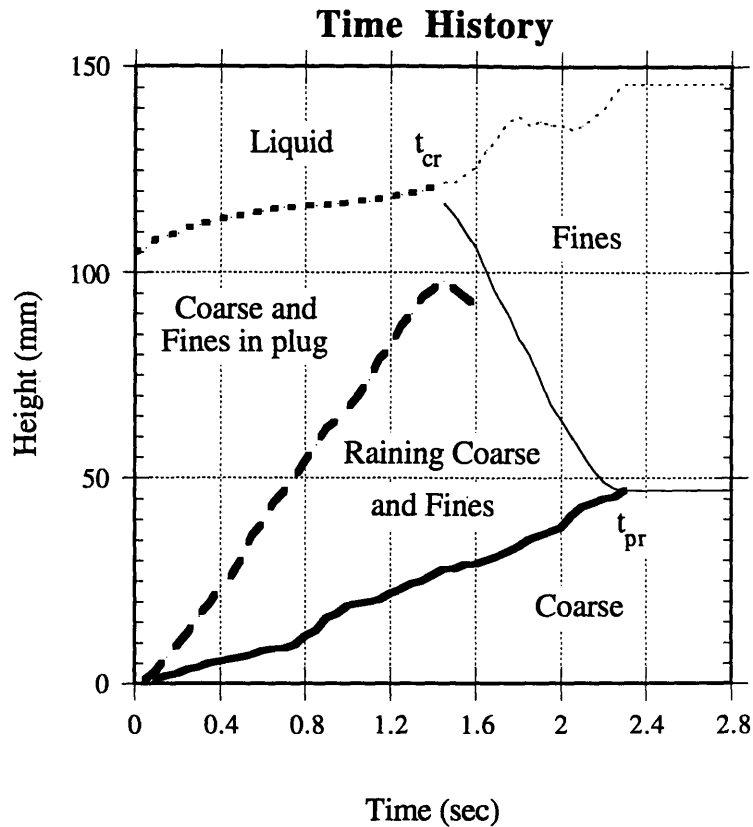


Figure 2-2: Time History.

evaluated at process time, t_{pr} , and (3) Maximum Segregation Process Height. Three dimensional plots for each of these dependent variables with the independent variables of final superficial velocity (Inlet Flow Rate divided by final test section cross-sectional area, Q_{li}/A_f) and Wall Velocity (V_w) are created. The 3-D plots cover a wide range of physically different phenomenon. In some cases, there was a smooth, slow expansion of the plug, ending in excellent fines removal. In other cases, the characteristic pocket or void hardly appeared to form and there was no net rise to the top of the plug, but a drop because the wall moved out so quickly. Here, removal was very poor. This experimental investigation provides further qualitative understanding of the physical phenomena. In general terms it explores how the reduction in volume and the mechanical jostling of the mixture brought on by the movable wall enhance the segregation process.

2.2 Experimental Apparatus

The experimental apparatus is shown in fig. 2-3. The tests occur in a rectangular plexiglass test section with one movable wall driven through a system of pulleys and no-slip belts powered by a variable speed motor. An impulsive flow is supplied by a positive displacement cylinder, filled with water and driven at constant speed by a variable speed motor. A time delay device was necessary to insure that the flow and wall start at the same time.

2.2.1 Positive Displacement Device

For the tests of impulsive segregation of a bi-disperse mixture between outwardly moving walls, a stepwise increase to the desired constant fluid flow rate was desired. This was provided by a positive displacement piston, driven at constant velocity so that the flow rate was independent of pressure drops in the circuit. The transient between no flow and constant flow conditions was short compared to the total test duration. A 1 hp Leeson variable speed motor with controller Minarik RG300 is connected through a gear box (ratio 20:1) to a driving screw mechanism. The screw drives a cylinder which drives water through the test section. The liquid is collected in an expansion tank at the exit of the test section.

The cylinder used is a Bimba 708DXP, having a piston cross sectional area of 5050 mm^2 . It is shown in fig. 2-3. The motor controller allows for a wide range of output flow rates for the cylinder (0 - $36,000 \text{ mm}^3/\text{s}$). The cylinder output flow rates have been calibrated against the motor controller setting, and this calibration curve is shown in fig. 2-4. The curve is linear. The flow reaches a nearly constant value in the time of 0.2 to 0.6 seconds compared to a typical test duration of 3 - 4 seconds.

2.2.2 Test Section Design and Construction

The general drawing of the experimental test section is shown in fig. 2-5, and the dimensioned drawing is in Appendix A. The test section is constructed from two pieces of 1.5 inch thick plexiglass stock which are milled out down the middle and

Experimental Apparatus

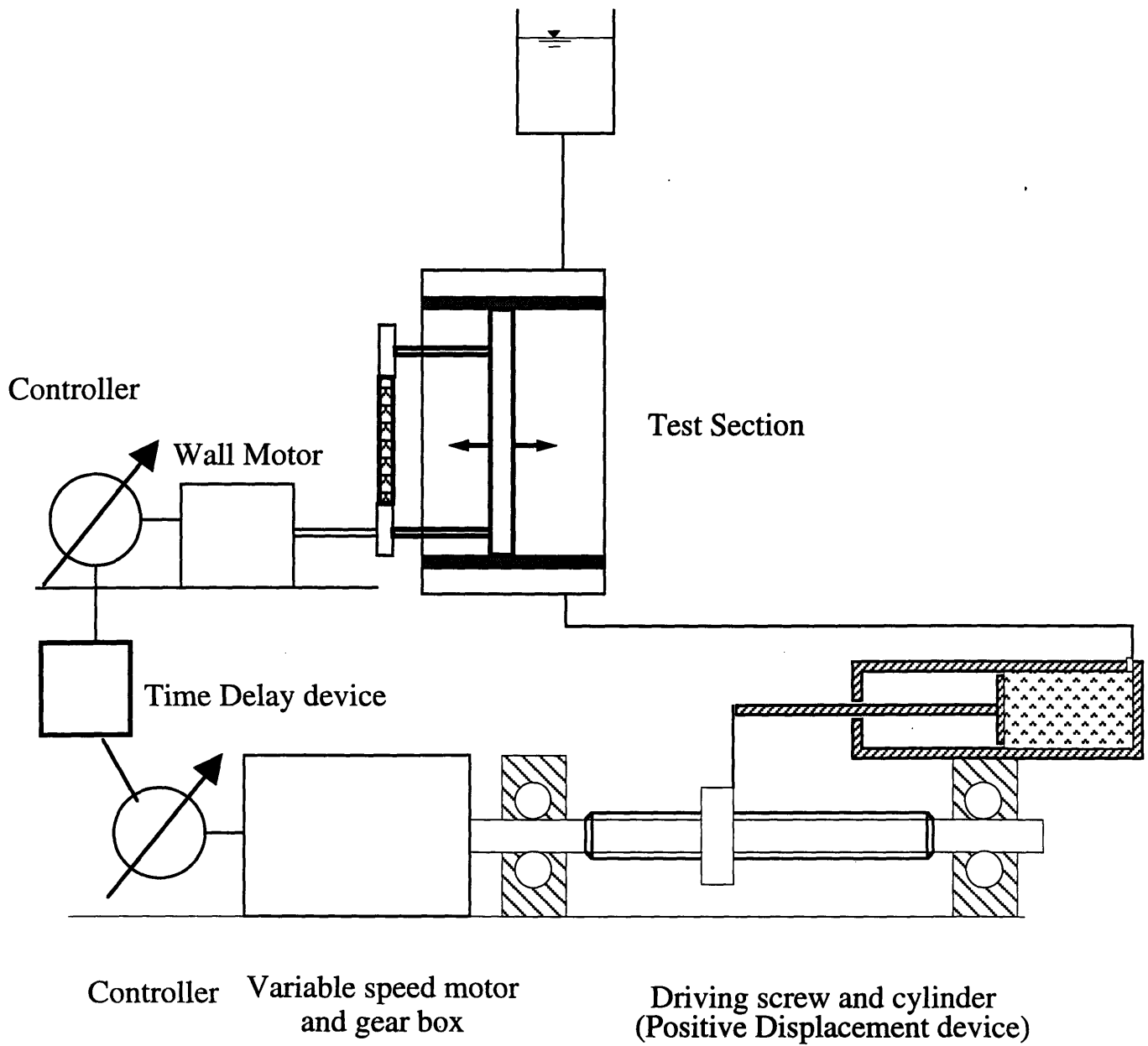


Figure 2-3: Experimental Apparatus.

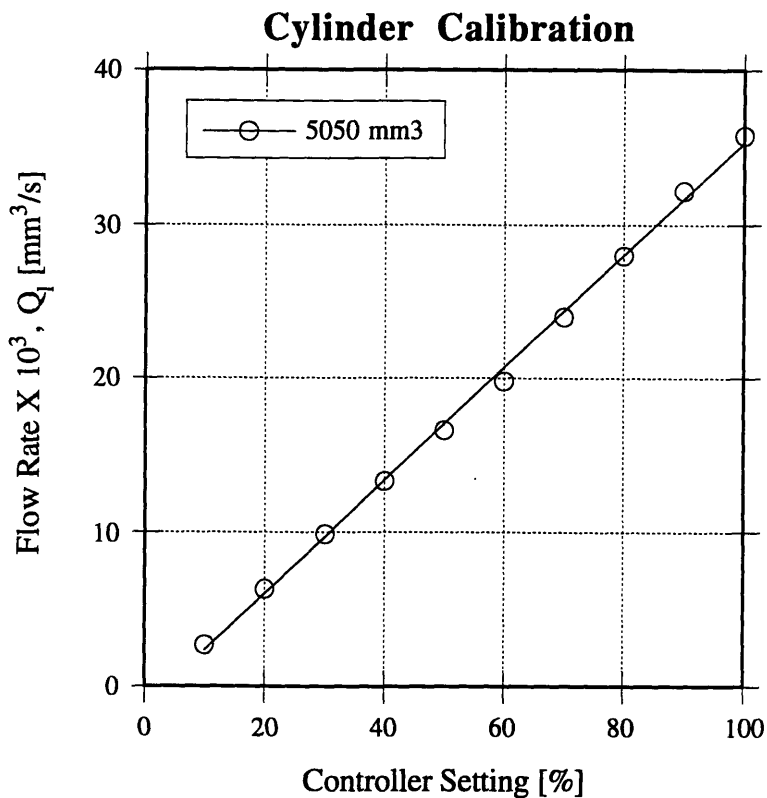


Figure 2-4: Cylinder Calibration.

capped at the ends by smaller pieces of plexiglass. The two test section halves are screwed tightly together, squeezing a 1/32 inch gum rubber gasket which is also pinched between the inner movable wall halves, A and B, made of plexiglass. Wall half A, as seen in fig. 2-6, has a thickness of 12.7 mm and has a 4 mm black rubber seal running around its edge. The black rubber seal is designed to keep the fine particles from creeping out of the bi-disperse mixture, but is not expected to prohibit passage of water. Wall half B is machined to attach to wall half A with four 8-32 1 inch nylon screws. Together, halves A and B pinch on the 1/32 inch gum rubber which acts as a diaphragm between the movable wall and the stationary housing to contain the water. The ends of half B are drilled so that 3/8 inch T-nuts may be installed. In these T-nuts are standard ASME 3/8 inch bolts, driven by the pulley system. This drives the movable wall. Within the test section, the movable wall isolates a channel which is the test chamber. The test chamber has a width of 40 mm and a thickness in the direction of wall motion of 10 to 18.5 mm. The height of the test volume is 160 mm. The ends of the test section are defined by two 1/4 inch high-density

Test Section (front view)

Test Section (side view)

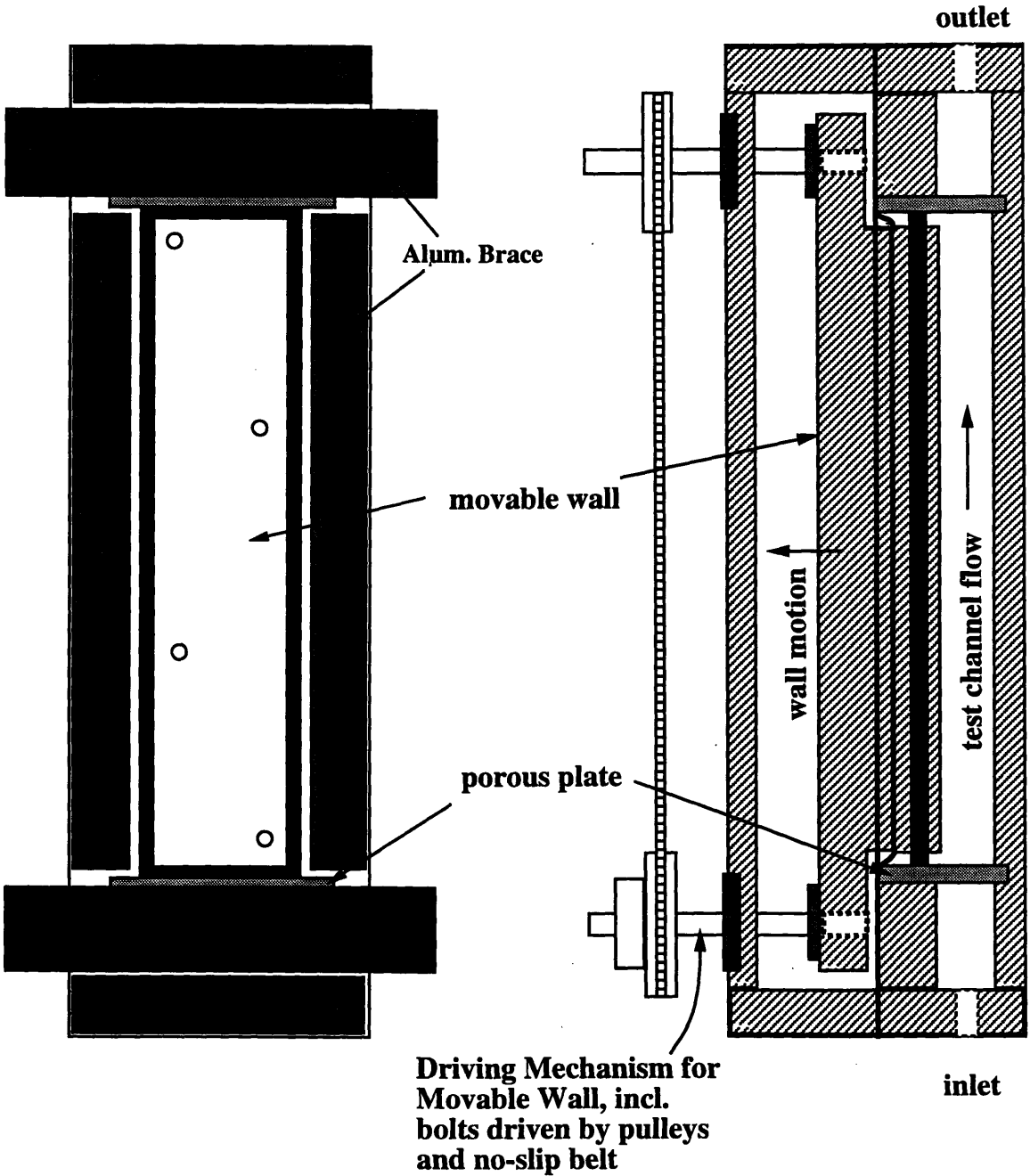
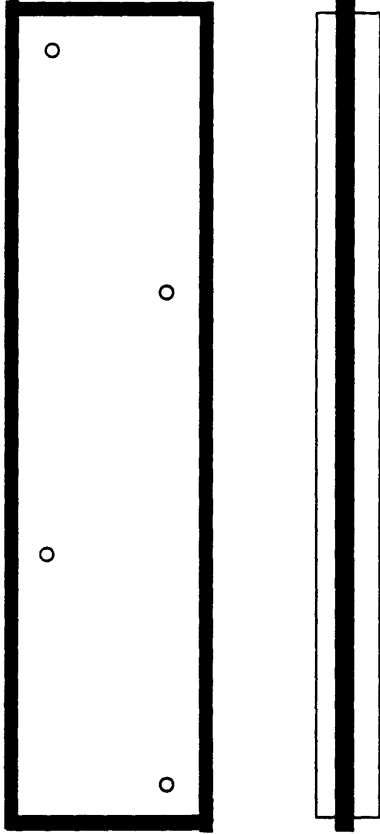


Figure 2-5: Test Section: front and side views.

Half A



Half B

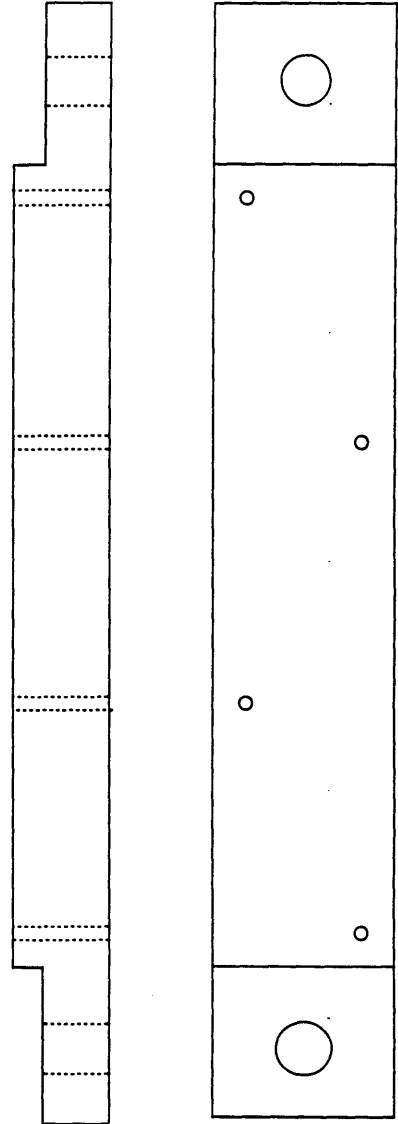


Figure 2-6: Test Section Wall Halves.

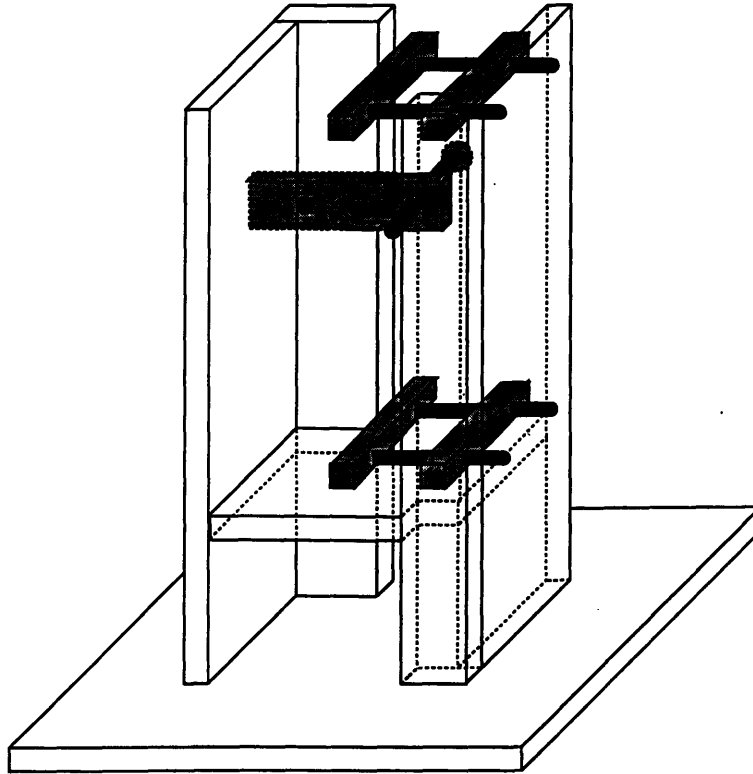


Figure 2-7: Test Section Holder.

polyethylene porous plates (Porex Technologies), having $60\mu\text{m}$ pore size. They are fitted at the top and bottom of the test section, and serve the purpose of preventing escape of the particles at the outlet and obtaining a uniform flow distribution across the test section at the inlet.

Holding the test section in place is a test section holder, fig. 2-7, constructed by gluing together $3/4$ inch plexiglass pieces with a chemical bonding compound. The holder is equipped with upper and lower systems of aluminum brackets to hold the test section firmly in place in a vertical upright position. In addition, the test section holder has an adjustable pulley which tightens the secondary no-slip belt as necessary. The secondary no-slip belt is connected to the upper and the lower test section pulleys, but not to the motor.

2.2.3 Movable Wall with Timing Belts and Pulleys

The movable wall is driven through a system of pulleys and no-slip timing belts. Observe from fig. 2-8, pulley A is first driven by a 1/8 hp Bodine motor connected to a Minarik speed controller. Pulley A then drives test section pulley B by way of the primary no-slip belt. Pulley B is fixed to pulley C. Pulley C is an element of the secondary no-slip belt system which is responsible for pulling the wall outward in a uniform, smooth way. The lower part of fig. 2-8 illustrates the driving mechanism for the movable wall, a symmetric system at the top and bottom of the test section. This driving mechanism is a brace to pinch the test section halves together and it holds the driving bolt as well. The driving bolt is a standard ASME bolt 3/8 inch in diameter, sitting in a bearing and fixed to rotational motion only so that the wall moves on it via the T-nut installed in wall half B. The bolts are driven by the pulley attached to the ends of each bolt.

Necessary for the experimental work was a wall calibration curve which has wall velocities in mm/s for given wall motor controller settings, fig. 2-9. It shows a nearly linear relationship, but often specific values of wall velocity were taken directly off the curve instead of applying the curve fitted equation. In this way, the best accuracy was obtained.

A microswitch served to stop motion of the wall so the wall did not contact the back of the test section. The switch was installed in the top of the test section, shutting off the power to the motor operating the system of pulleys and driving the wall when engaged by the moving wall. A variable time delay device was wired in the system to insure wall motion and flow rate begin at the same time.

2.3 Experimental Measurement Tools

2.3.1 Image Analysis System

The experimental work relied heavily on an image analysis system to quantify variables describing the behavior of the bi-disperse mixture. Image analysis proves to be

Pulley and No-slip Belt System

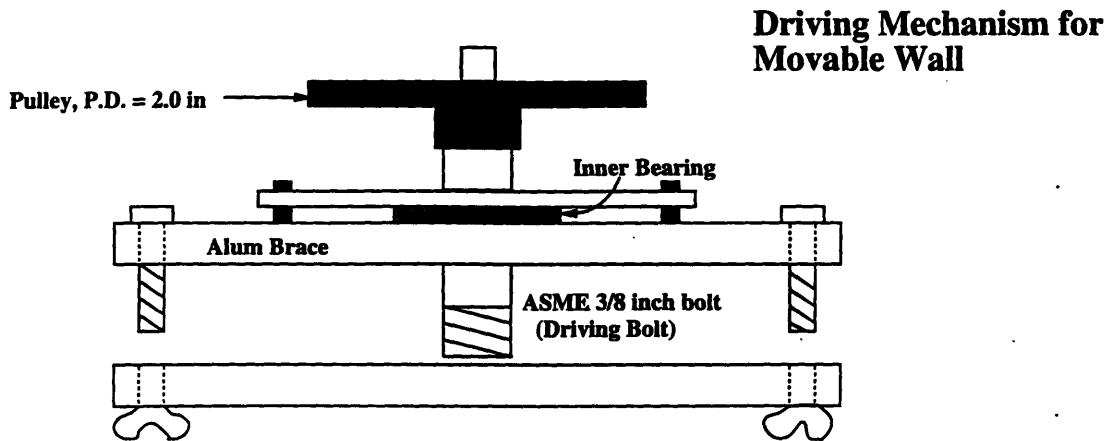
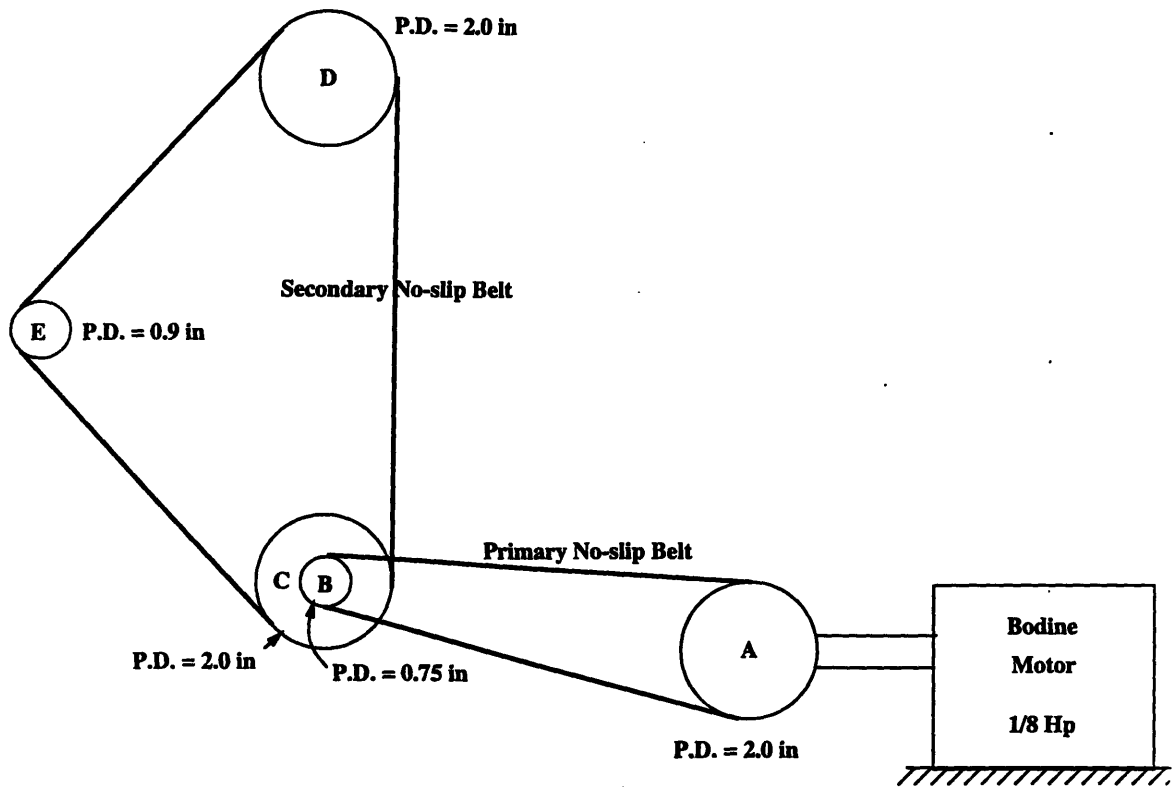


Figure 2-8: Pulley and No-Slip Belt System and Driving Mechanism for Movable Wall.

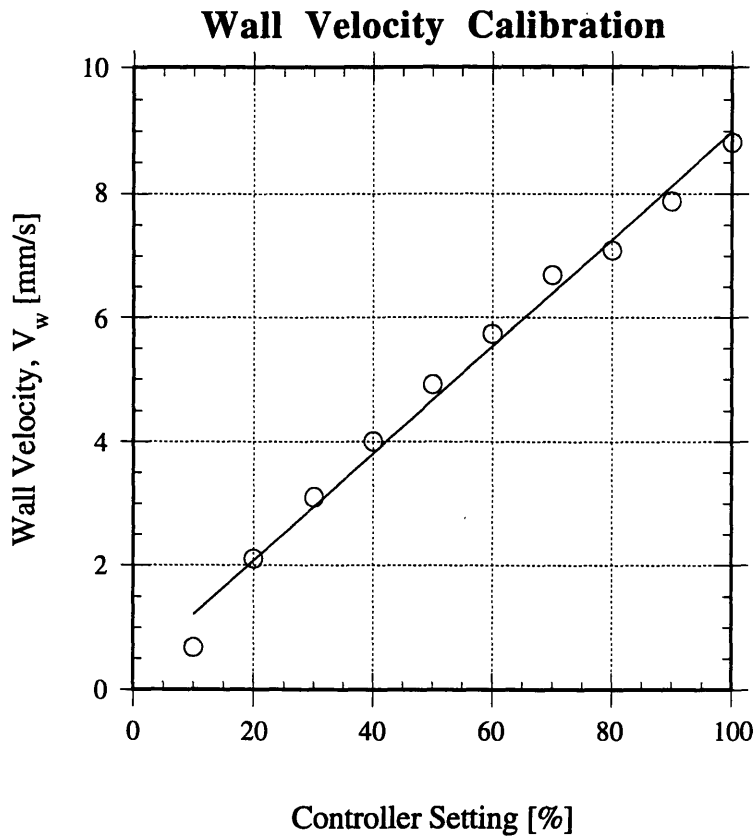


Figure 2-9: Wall Velocity Calibration.

a powerful and insightful tool as it provides immediate physical insight of the physical phenomena involved, and it allows images to be enhanced through brightness and contrast controls in a desirable way so the quantitative information may be extracted. The quantities which are measured are species concentration, height of the bed, and significant times in the experiment. Species concentration is measured through a luminance versus fines concentration calibration curve for maximum and minimum test section thicknesses. That is, from the measured luminance of a region of interest, a fines concentration value can be inferred. Significant times, like process time, t_{pr} , are determined visually using a frame-by-frame advance dial on the VCR.

Fig. 2-10 illustrates a schematic of the image analysis system. The test section is back-illuminated with a fluorescent light covered with a diffuser. A CCD video camera (Panasonic PK-958) is connected to a SVHS VCR (video-cassette-recorder) Panasonic AG-7355. The SVHS standard has better resolution compared to the traditional VHS standard - more than 400 lines per screen, as opposed to only 240 lines per screen. The VCR has the capability to access the images recorded on tape

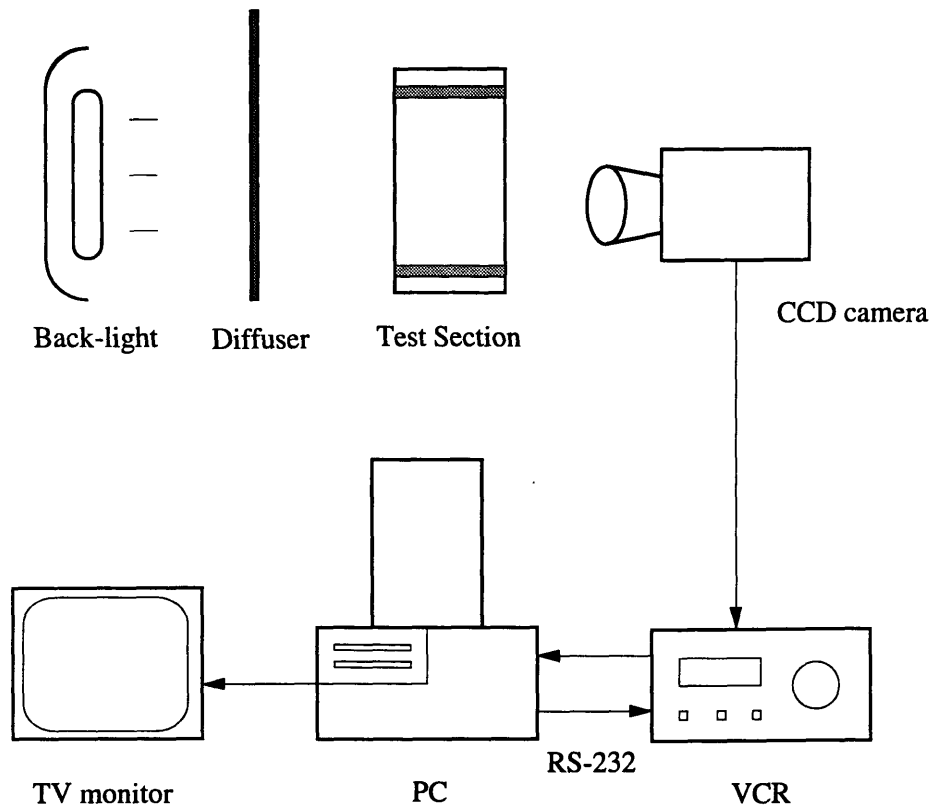


Figure 2-10: Schematic of the image analysis system.

field by field, or every 1/60th of a second. Two successive fields compose a frame which occur every 1/30th of a second. Each frame can be paused and frozen on a digital memory internal to the VCR. The VCR has the interface board AG-IA232TC for serial standard RS-232 communication. This enables the VCR to be completely controlled by a PC; the VCR is interfaced with an Austin PC Intel 486 (33 MHz and 350 MB hard disk to provide for adequate speed and storage memory support). A frame grabber board ITI-OFG-640 (Image Technology. Overlay Frame Grabber) is installed on the PC for image digitization. The frame grabber is a 12-bit device, with the first 8 bits used to create a 256 gray value image, and the remaining 4 bits used for text and overlay. The frame grabber can store images up to 640 X 480 pixels in size. No more than one image at a time can be stored on the frame grabber. The frame grabber displays the image on a TV monitor, or on the PC.

The PC needs image processing software to work with the images through the VCR and frame grabber board. The package used is Optimas version 3.1, developed by BioScan Corporation. We programmed Optimas, which support ALI (Analytical

Language for Images), a C-based language, to perform several tasks. For example, we had Optimas acquire a sequence of images, enhance those images, and store them on memory. We also programmed Optimas to measure luminance values from which fines concentration values of the bi-disperse mixture were inferred. Schiaffino [1993] did a large portion of the programming.

2.3.2 Luminance vs. Fines Concentration Calibration Curve for Minimum and Maximum Test Section Thicknesses

In order to quantify the value of Fines Removal Fraction at process time, t_{pr} , it is necessary to have a Luminance vs. Fines Concentration Calibration Curve for Minimum and Maximum Test Section Thicknesses. Schiaffino found that the luminance values of an image can be related to the fine particle concentration in the test section. The higher the concentration of the fines, the darker the region appears and the lower the luminance reading. Schiaffino obtained a calibration curve from images for steady fluidization cases, where the fines are homogeneously fluidized to a known concentration value in a coarse matrix between fixed walls. He found that his experimental points fit an exponential curve which is a common best fit curve in attenuation problems. This process was adopted in developing the Luminance vs. Fines Concentration Calibration Curve for Minimum and Maximum Test Section Thicknesses, shown in fig. 2-11. These curves are created for the region of interest bounded by the sides of the test section, by the porous plate on the bottom, and by the upper interface of the coarse matrix where the remaining coarse particle lands at process time, t_{pr} . Schiaffino confirmed through a study of the dependence of luminance readings on test section thickness that it is necessary to have a test section thickness greater than three times the coarse particle diameter for accurate results. Since this experiment's coarse particles were 3.0 mm, and test section width ranged from 10 mm to 18 mm, sufficient accuracy was obtained.

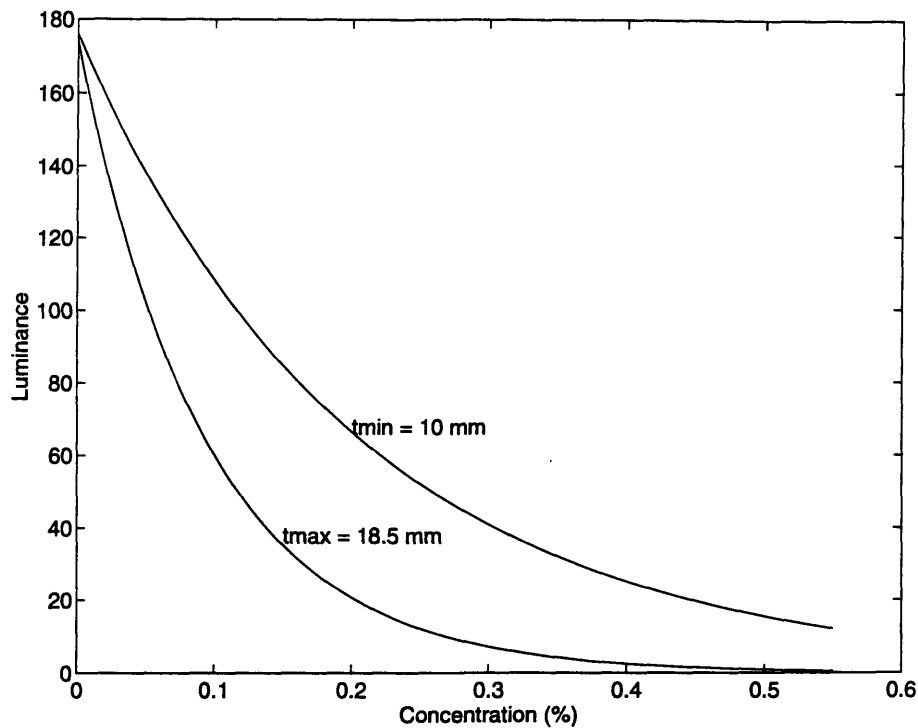


Figure 2-11: Luminance vs. Fines Concentration Calibration Curve for Minimum and Maximum Test Section Thicknesses.

2.4 System Characterization: Step Wall and Step Flow Tests

Determination of the system time delays and the behavior of the flow and wall motion in time was determined through a step wall motion and step flow rate test performed in the test section with liquid only. Results of the test are in fig. 2-12. This shows Outlet Liquid Displacement and Wall Displacement in time for the Inlet Flow Rate of $Q_{li} = 31,500 \text{ mm}^3/\text{s}$ and the Wall Velocity of $V_w = 2.2 \text{ mm/s}$. The procedure in obtaining this plot was to plug the positive displacement device motor and the wall motor into the same outlet, along with an electric light bulb. The outlet was turned on, and time zero was set as the time when the electric light went on. A video camera captured the light bulb, a side view of the test section with its movable wall, and a graduate cylinder on the outside of the test section, connected to the outlet of the test section. From a frame-by-frame analysis of the sequence of video images, Outlet

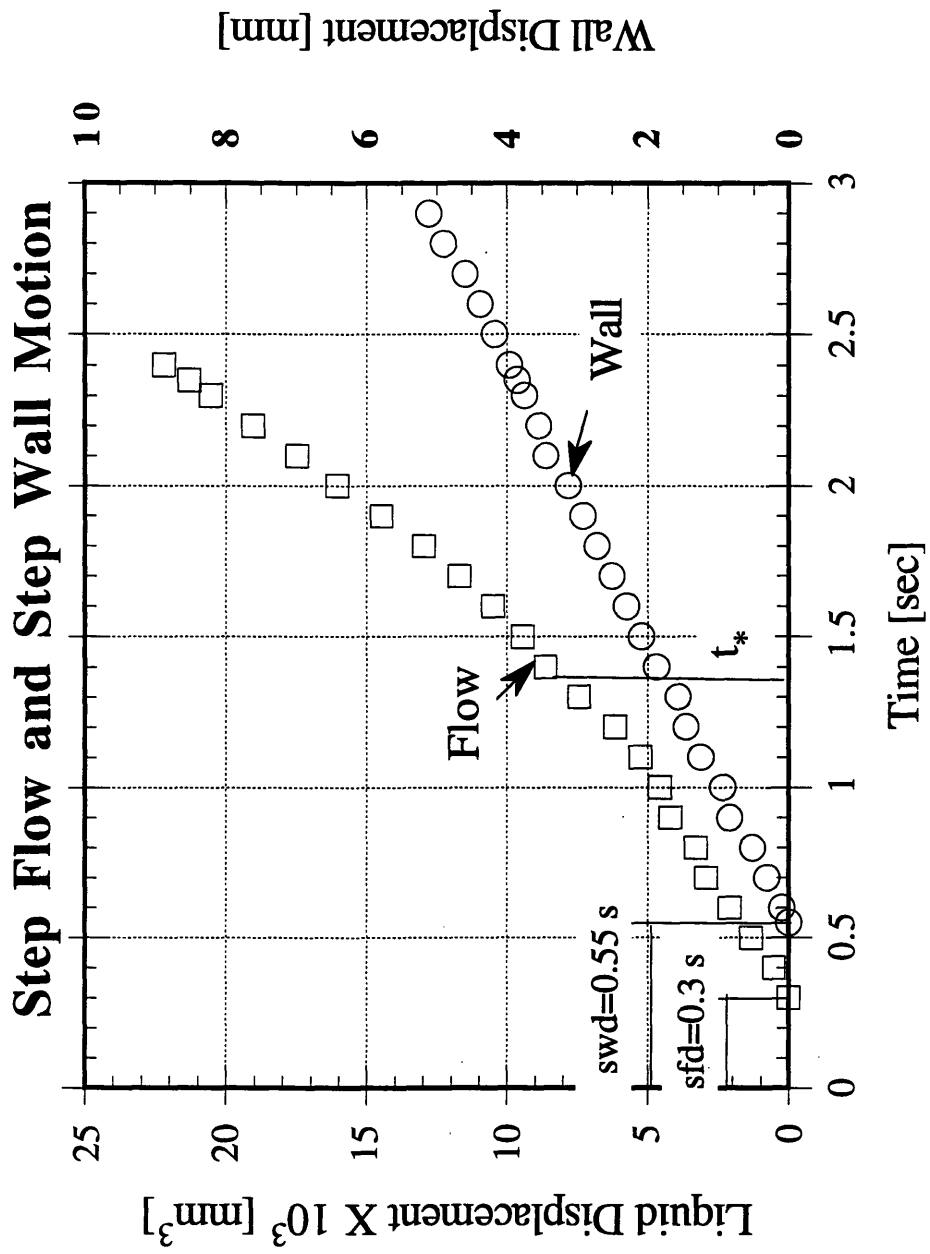


Figure 2-12: Step Flow and Step Wall Motion.

Liquid Displacement and Wall Displacement were recorded in time. System time delays for flow and wall motion were taken as the time their respective actions began after time zero. According to this plot, a system flow delay of 0.3 seconds, and a system wall delay of 0.55 seconds were characteristic of the experimental setup. This means it was necessary to input a flow delay of 0.25 seconds to the experimental runs to make the flow and wall start at the same time. Note also from the plot that the wall moves out evenly in time. That is, the Wall Velocity, or the slope of this Wall Displacement in time line is constant. However, the Liquid Displacement in time line has a “kink” in it at t_* , revealing that there is some compliance in the system. That is, the outlet liquid flow rate (the slope of the Liquid Displacement line in time) is lower at $Q_{lo} = 6,700 \text{ mm}^3/\text{s}$ up to the time of approximately 1.35 seconds and then takes a sudden jump to $Q_{lo} = 14,700 \text{ mm}^3/\text{s}$. This is because some liquid flow is lost to a “pocket” in the test section, with the Flow Rate jumping to a higher value once the “pocket” is filled. Filling of the pocket is thus identical to an increased outward displacement of the wall in terms of its influence on fluid velocity. It is believed that the pocket is in the upper and lower regions of the 1/32 inch gum rubber seal, behind the T-nuts. Note this test was run at an Inlet Flow Rate of $Q_{li} = 31,500 \text{ mm}^3/\text{s}$ and Wall Velocity, $V_w = 2.2 \text{ mm/s}$, and t_* will be different for other combinations of Q_{li} and V_w .

The presence of a “kink” at t_* has shown up in repeated tests with this Q_{li} , V_w combination. Also, unfortunately, t_* occurs within the runs of many of our experiments which last about 3 - 4 seconds. For this Inlet Flow Rate up to t_* , outlet liquid superficial velocities decrease from 16.8 mm/s to 14 mm/s (at t_*) because of the outwardly moving wall. After t_* , outlet liquid superficial velocities vary from 30.6 mm/s (at t_*) to 19.9 mm/s at the end of the wall motion, whereupon it jumps to 42.6 mm/s when the wall motion stops. There is a significant step in outlet liquid superficial velocity at t_* , from 14 mm/s to 30.6 mm/s, a 120% increase. Note that the increase of outlet liquid superficial velocity upon cessation of wall motion to 42.6 mm/s from 19.9 mm/s (115%) is a similar percentage. This may be a little deceiving however, as the outlet liquid superficial velocity is less than the liquid superficial velocity at

the region of experimental interest in the test section, and a “kink” or step in flow rate may not be as great a factor in the results as previously thought. By continuity, the effect of an outward wall motion is a linearly decreasing liquid velocity as one moves upward between the diverging walls. The liquid velocity at the bottom of the test section is affected by the wall position, of course, but not by the Wall Velocity. Liquid velocity is further affected at heights of experimental interest by the fact that the test chamber volume is increasing. The effect of Wall Velocity thus increases linearly with distance from the bottom. Depending on the specific test conditions, ie Q_{li} , V_w combination, much of the segregation process occurs in a range where the decreasing fluid velocity may be of some influence. However, the original liquid superficial velocity, and the liquid superficial velocity after the step are always greater than the terminal velocity of the fine particles, and less than the terminal velocity of the coarse particles, so that the most necessary requirement of fine particle removal remains. A systematic investigation of how the step in flow rate at t_* changes the behavior of the segregation process should be done.

2.5 Seven Experimental Parameters

The seven important parameters, or main characteristics for this experimental investigation are listed in Table 2.1. The Coarse and Fine particle sizes, d_c and d_f , are comparable to those used in Schiaffino’s work, and are also chosen based on their availability and on their behavior under the given flow and wall motion conditions. The Bed Height, h , could be anything from the minimum reasonable value of 40 mm (which is the test section width) up to the maximum test section height of 160 mm. Wall Displacement, d_w , covers the range of 0 to 8.5 mm. That is, the chamber width may vary from 10 to 18.5 mm, a reasonable range for varying the gap of a crushing device. Wall Velocities, V_w , fell in the range of 0 to 8.5 mm/s. Expanding this range would require a more powerful motor. The Inlet Flow Rate range $Q_{li} = 0$ to 36,000 mm³/s is dictated by the size of the cylinder. The 1 hp motor driving the cylinder is definitely powerful enough to drive this cylinder or a larger one, but the chosen

Parameter	Range
Coarse Particle Diameter, d_c	0.2-0.4 mm
Fine Particle Diameter, d_f	2-5 mm
Bed Height, h_o	40-160 mm
Wall Displacement, d_w	0-8.5 mm/s
Wall Velocity, V_w	0-8.5 mm/s
Flow Rate, Q_I	0-36,000 mm ³ /s
Wall or Flow Delay	0.05-2.0 s

Table 2.1: Seven Experimental Parameters

cylinder works well with the other experimental parameters such as the Wall Velocity. That is, knowing the diverse physical phenomena in the experiments possible, the Inlet Flow Rate and Wall Velocity ranges cover the phenomena well for an initial investigation.

Since this experimental investigation is the study of the fluidized mechanical segregation process, the parameters to vary are Inlet Flow Rate and Wall Velocity. Parameters such as Coarse and Fine Particle diameters and Bed Height are characteristics of a crushing process in a machine. That is, their characteristics are a result of the method of crushing and the design of the machine. The Time Delay Device's function is only to input a flow delay so that startup of Flow Rate and wall motion occur at the same instant in time. In further experiments, it may be interesting to investigate if slight delays in startup between the flow and wall motion in any way improve the segregation process. At the moment, we are investigating tests with simultaneous flow and wall delay motion.

2.6 Data Collection: Experimental Planar Plot

Fig. 2-13, the Experimental Planar Plot, maps the field of experimental points, or the combinations of Inlet Flow Rate, Q_{li} , and Wall Velocity, V_w , where 18 tests were run. These were chosen to investigate the range of physical phenomena available to this apparatus. For example, it is obvious that point 3, shown in fig. 2-14 with low V_w and high Q_{li} , differs greatly from point 6, shown in fig. 2-15 with high V_w and low Q_{li} . Point 3 shows the plug rising to a relatively high height. The segregation process takes time, but overall fine particle removal is excellent. Point 6 has poorer fine particle removal, but occurs very quickly. Note the top of the bed in this latter case, as contrasted to the rising plug in the former.

The Experimental Planar Plot shown in fig. 2-13 has a line indicating where superficial fluid velocity at the bottom of the test section equals the terminal velocity of the fine particles of diameter 0.2 mm. This last line is tied to Schiaffino's work, discussed in section 1.4.2. By continuity, the effect of an outward wall motion is a linearly decreasing fluid velocity as one moves upward between the diverging walls. Multiplying $j_l = U_\infty$ of the fines at the bottom of the test section by maximum test section cross-sectional area (40 mm X 18.5 mm) as an upper limit estimate, the inlet flow necessary for clearing the fines, 17,600 mm³/s, is obtained. This line corresponds to the point on Schiaffino's plot of Fines Removal Fraction, fig. 1-21, where Fines Removal improves dramatically. It can be expected, then, that tests taken to the right of this line, such as 2, 3, 5, etc. should show high removal fractions (>80%). Those to the left of the line should have poorer removal fractions.

The second line is the line of constant height of the mixture during the fluidized segregation process. Above this line, the top of the mixture should fall below its original height, h_o , during the fluidized mechanical segregation process; below this line, the top of the mixture should rise above its original height. The line of constant height is determined by equating two top of the plug velocities, U_{t1} and U_{t2} . The first velocity of the top of the plug, U_{t1} , is determined as a function of Wall Velocity, V_w , for the case of the mixture subject to no upward flow, and opened up with a

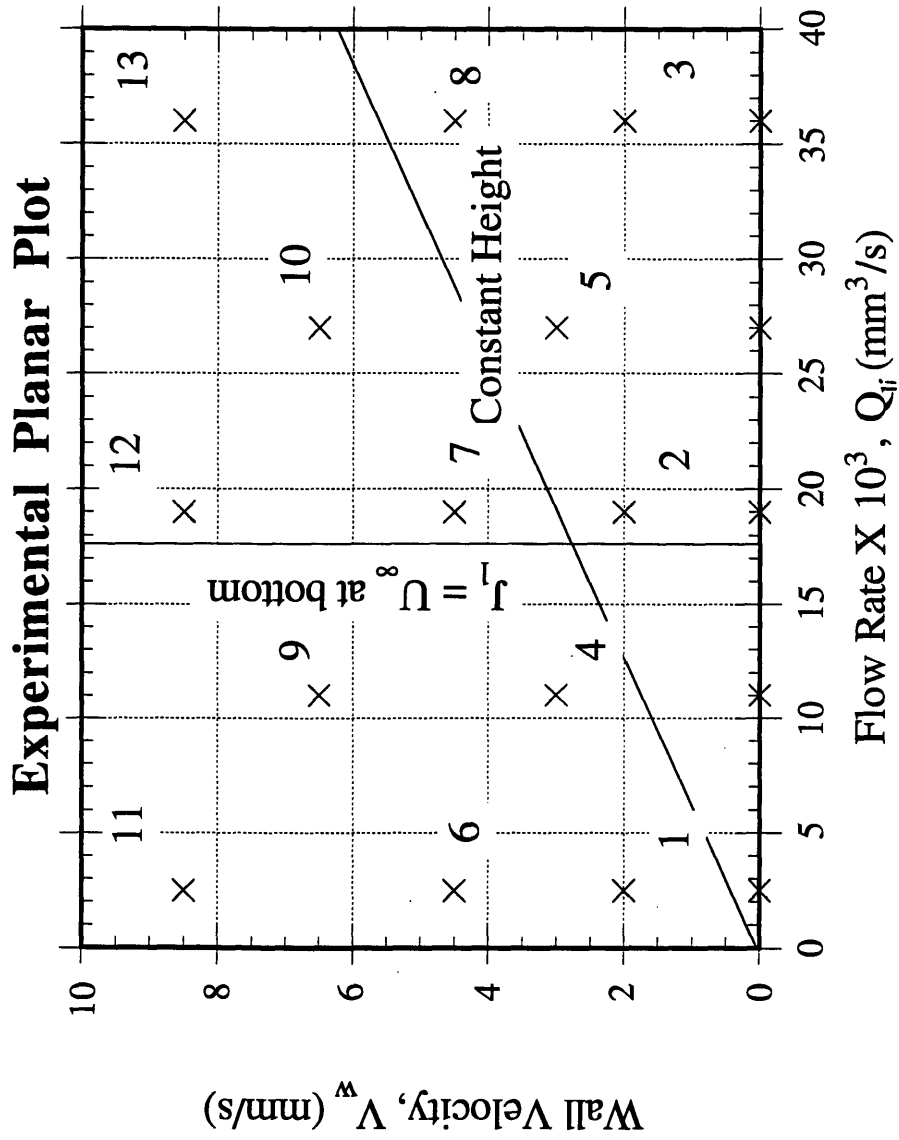


Figure 2-13: Experimental Planar Plot.

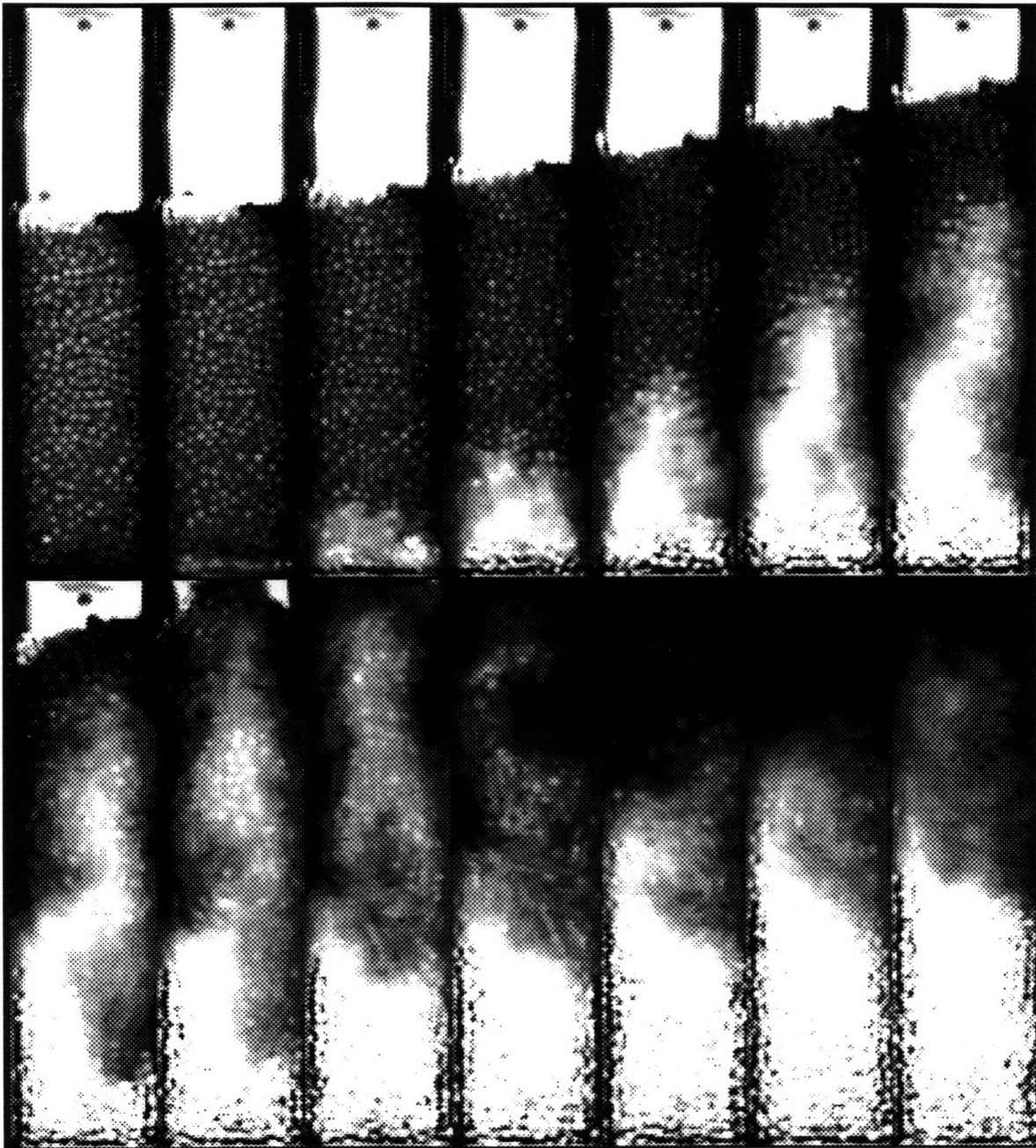


Figure 2-14: Point 3: Low $V_w = 2.0$ mm/s, High $Q_{li} = 36,000$ mm³/s. (frames spaced 1/6th second).

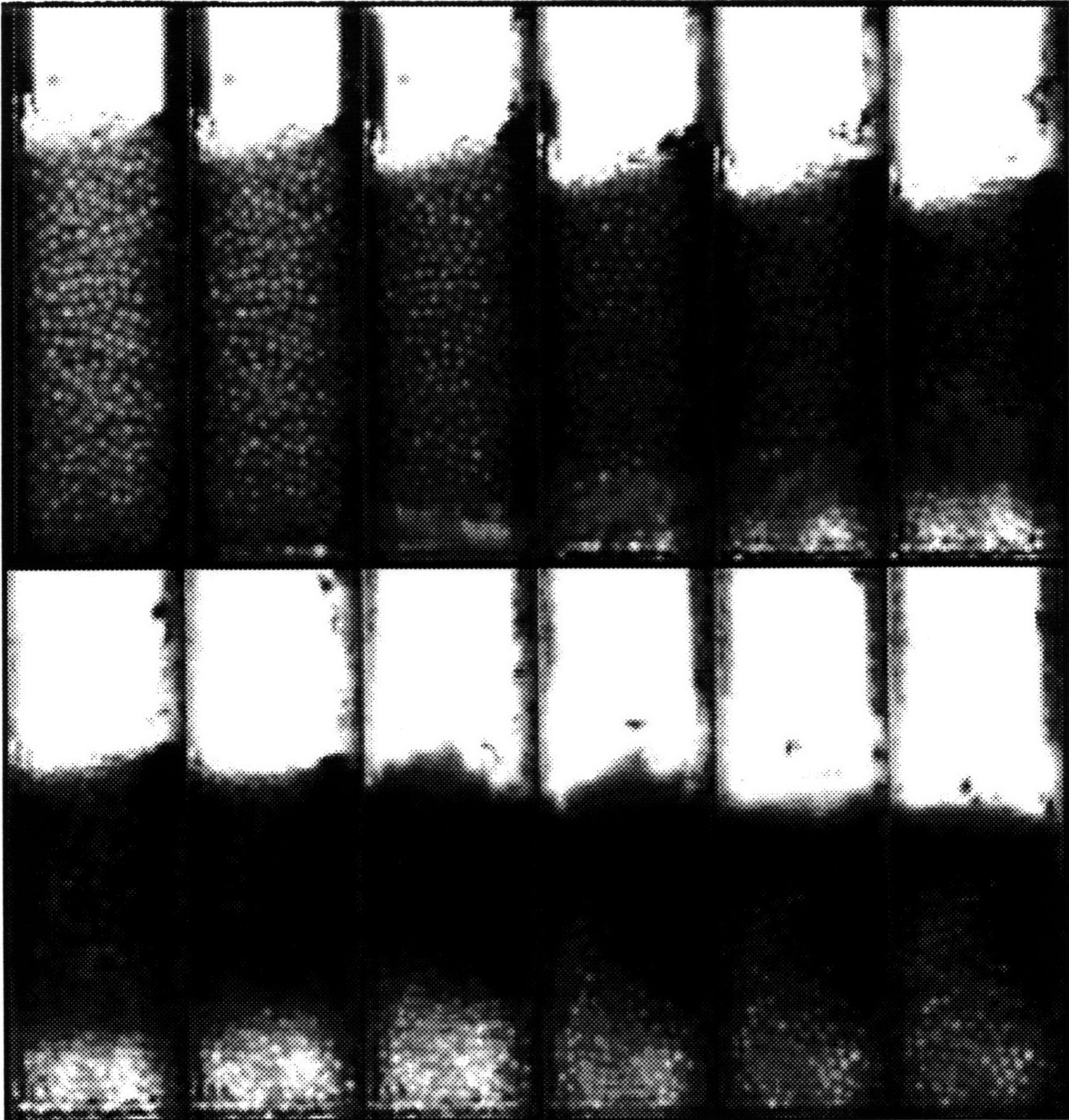


Figure 2-15: Point 6: High $V_w = 4.5$ mm/s, Low $Q_{li} = 2500$ mm³/s. (frames spaced 1/6th second).

Wall Velocity, V_w . The second velocity of the top of the plug, U_{t2} , is determined from Schiaffino's work, fig. 1-17, a plot of Upward Bed Velocity, U_t , versus liquid superficial velocity, j_l . Measuring the slope of the line on the plot gives Upward Bed Velocity, U_t , as a function of liquid superficial velocity, j_l . This is converted to Upward Bed Velocity, U_t , as a function of Inlet Flow Rate, Q_l , and this is called U_{t2} . Finally, equating U_{t1} and U_{t2} results in an equation relating V_w and Q_l . This equation is plotted as the line of constant height on the Experimental Planar Plot, fig. 2-13.

Design questions can be addressed based on the 18 tests outlined on the experimental planar plot. Three-dimensional plots having three measured design criteria of (1) Clearing Speed, defined as final bed height divided by process time, h_f/t_{pr} , (2) Fines Removal Fraction at process time, t_{pr} , and (3) Maximum Height of the fluidized segregation process as dependent variables have been developed. The independent variables are Wall Velocity, V_w , and Final Superficial Fluid Velocity (Inlet Flow Rate divided by final test section cross-sectional area), Q_{li}/A_f . All three measured criterion serve as useful design criterion. Clearing Speed is an important design criterion, as higher Clearing Speed means crushing cycles can be run at higher frequency which translates into a higher production rate of crushed products. Fines Removal Fraction is a measure of the efficiency of the process. More fines in the remaining coarse material inhibits breakage in the next crushing cycle, also slowing production. Lastly, Maximum Height of the process is important because it represents how much space is needed for the removal process. The less the space required, the smaller the machine necessary and the less the tendency to prematurely discharge coarse material. A smaller machine translates into a lower machine cost. The 3-D plots are shown in figs 2-16, 2-22, and 2-23. Figs 2-16 and 2-22 have a set of 18 points, including five representing the condition of zero wall velocity at maximum test section cross-sectional area (40 mm X 18.5 mm). These correspond to the static wall conditions explored by Schiaffino.

2.7 Results and Discussion

Following is a qualitative discussion of the physical phenomenon seen in the 13 tests with Q_{li} , V_w combinations, and notes on the three design-criterion and what their 3-D plots reveal about the physical phenomena seen in experimental tests.

2.7.1 Qualitative Discussion of the Physical Phenomenon in the 13 Tests

As stated before, selecting specific Q_{li} , V_w combinations within the wide range of Inlet Flow Rates (2500 - 36,000 mm³/s) and Wall Velocities (0 - 8.5 mm/s) allows for a large diversity of physical phenomenon to be viewed. This discussion details the specifics of the segregation processes of the 13 tests with Q_{li} , V_w combinations.

Test 1 ($Q_{li} = 2500$ mm³/s, $V_w = 2.0$ mm/s) has very little pocket formation, just a slight wave moving upwards. Some, but definitely not all fine particles percolate gently through with the wave. There is no back mixing of fine particles, no channeling of upflow, and no swirl. Breakthrough is not violent. Test 2 ($Q_{li} = 19,000$ mm³/s, $V_w = 2.0$ mm/s) is more dynamic. The pocket meanders up through the plug, with channeling of upflow occurring on the left initially, then switching to channeling on the right side. The result of this is fine particles trapped within the mixture, and a big counter-clockwise swirl at plug breakthrough. There is little back mixing of fine particles at plug breakage as the high flow rate pushes them upward. Test 3 ($Q_{li} = 36,000$ mm³/s, $V_w = 2.0$ mm/s) features the extreme high in Inlet Flow Rate, and the extreme low in Wall Velocity. There was a smooth, evenly formed pocket halfway up, then a channeling of upflow to the right side, causing a very large counter-clockwise swirl at breakthrough at a high height in the test section. Fine particles find their way through efficiently because the flow rate is so high. There is no back mixing of fine particles at the end. Test 4 ($Q_{li} = 11,000$ mm³/s, $V_w = 3.0$ mm/s) has a clearly defined pocket all the way up with no channeling. A clean breakthrough occurs in the center of the plug. Fine particles sweep out with the pocket, but not completely. Some are left behind. There is no back mixing and no swirl. Test 5 ($Q_{li} = 27,000$

mm³/s, $V_w = 3.0$ mm/s) has a clearly defined pocket the whole way up, and fine particles migrate through almost completely with the wave. There is no channeling of upflow, and there is a clean break in the center of the plug at the end. There is a small clockwise swirl, but no back mixing of fine particles. Test 6 ($Q_{li} = 2500$ mm³/s, $V_w = 4.5$ mm/s) shows little of a pocket formed. In this quick process, coarse move downward, and there is insufficient fluid velocity to effectively clear the fines. Fines removal is poor. The plug breaks in the center. There is no channeling of upflow, no swirl, and no back mixing of fine particles. Test 7 ($Q_{li} = 19,000$ mm³/s, $V_w = 4.5$ mm/s) is very similar to Test 6, but a larger pocket is formed and there is a better sweeping out of fine particles. The plug breaks in the center. There is no channeling of upflow, no swirl, and no back mixing of fine particles. Test 8 ($Q_{li} = 36,000$ mm³/s, $V_w = 4.5$ mm/s) shows clean pocket formation for two-thirds of the pocket's travel, followed by strong channeling on the left side, so there is a big clockwise swirl at the end which causes back mixing of fine particles. Eventually, those fine particles pulled down into the coarse are swept out by the strong flow. Test 9 ($Q_{li} = 11,000$ mm³/s, $V_w = 6.5$ mm/s) has a clearly defined pocket all the way up with no channeling. A clean breakthrough occurs in the center of the plug. Fine particles sweep out with the pocket, but not completely. Some are left behind. There is no back mixing and no swirl. Test 10 ($Q_{li} = 27,000$ mm³/s, $V_w = 6.5$ mm/s) has a clearly defined pocket most of the way up, but some channeling on the left side and clockwise swirl at the end. Fine particles migrate through almost completely with the wave. There is no back mixing of fine particles. Test 11 ($Q_{li} = 2500$ mm³/s, $V_w = 8.5$ mm/s) has a clean pocket with a little channeling on the left side. Fines do not sweep out very well under these conditions of extreme low Inlet Flow Rate and extreme high Wall Velocity. There was no swirl and no back mixing of fine particles. Test 12 ($Q_{li} = 19,000$ mm³/s, $V_w = 8.5$ mm/s) occurs quickly. There is a clean pocket formed, and a quick breakthrough in the center of the plug. Fine particle removal is good. Some clockwise swirl is present, and a little back mixing of fine particles. Fine particles percolate through the coarse matrix after the coarse have settled. Test 13 ($Q_{li} = 36,000$ mm³/s, $V_w = 8.5$ mm/s) is the case of extreme highs in Inlet Flow Rate and

Wall Velocity. The segregation process occurs very quickly. A clean pocket forms quickly and lasts two-thirds of the way up. There is then a slight channeling on the right side, and a resulting counter-clockwise swirl at breakthrough. There is some back mixing of fine particles, but all are eventually removed by the high flow rate.

2.7.2 Clearing Speed

Fig. 2-16 shows Clearing Speed, taken as final bed height divided by process time, h_f/t_{pr} , versus Wall Velocity, V_w , and Final Superficial Fluid Velocity (Inlet Flow Rate divided by final test section cross-sectional area), Q_{li}/A_f . Recall that process time, t_{pr} , refers to the instant during the fluidized mechanical segregation process when the final coarse particles from the broken plug settle to the pile of cleared coarse on the bottom. t_{pr} is illustrated earlier in figs. 2-1 and 2-2. Final bed height, h_f , is the height of the settled clear coarse matrix after the wall has moved out. For all of these tests, with a constant charge of material, it was 54 mm.

From fig. 2-16, note that the curve at zero Wall Velocity and maximum test section cross-sectional area agrees with Schiaffino's results for impulsive flow of a mixture in a constant cross-sectional area rectangular test section: segregation or clearing speed increases with flow rate. To illustrate this, Schiaffino's values from fig. 1-19 are plotted as a dashed line in fig. 2-16. This test and Schiaffino's test were run in similar, though not identical, rectangular constant cross-section test sections. Schiaffino has shown that cross-sectional area does not affect the clearing speed over the range of test conditions given in fig. 1-19.

It is obvious from fig. 2-16 that Wall Velocity has a greater affect on Clearing Speed than Inlet Flow Rate. Higher Wall Velocity results in a higher Clearing Speed. This is due to the fact that the wall moves out quickly, creating volume so that the plug spreads laterally and descends quickly. Put another way, the faster the wall moves out, the greater is the measured Depletion Velocity of the plug, $U_{dep} = U_b - U_t$, which is related to the Clearing Speed. Fig. 2-17 illustrates a 3-D plot of measured Depletion Velocity for the 18 tests. U_b refers to the bottom of the plug. U_t refers to the top of the plug. Both were experimentally observed from video images. Except

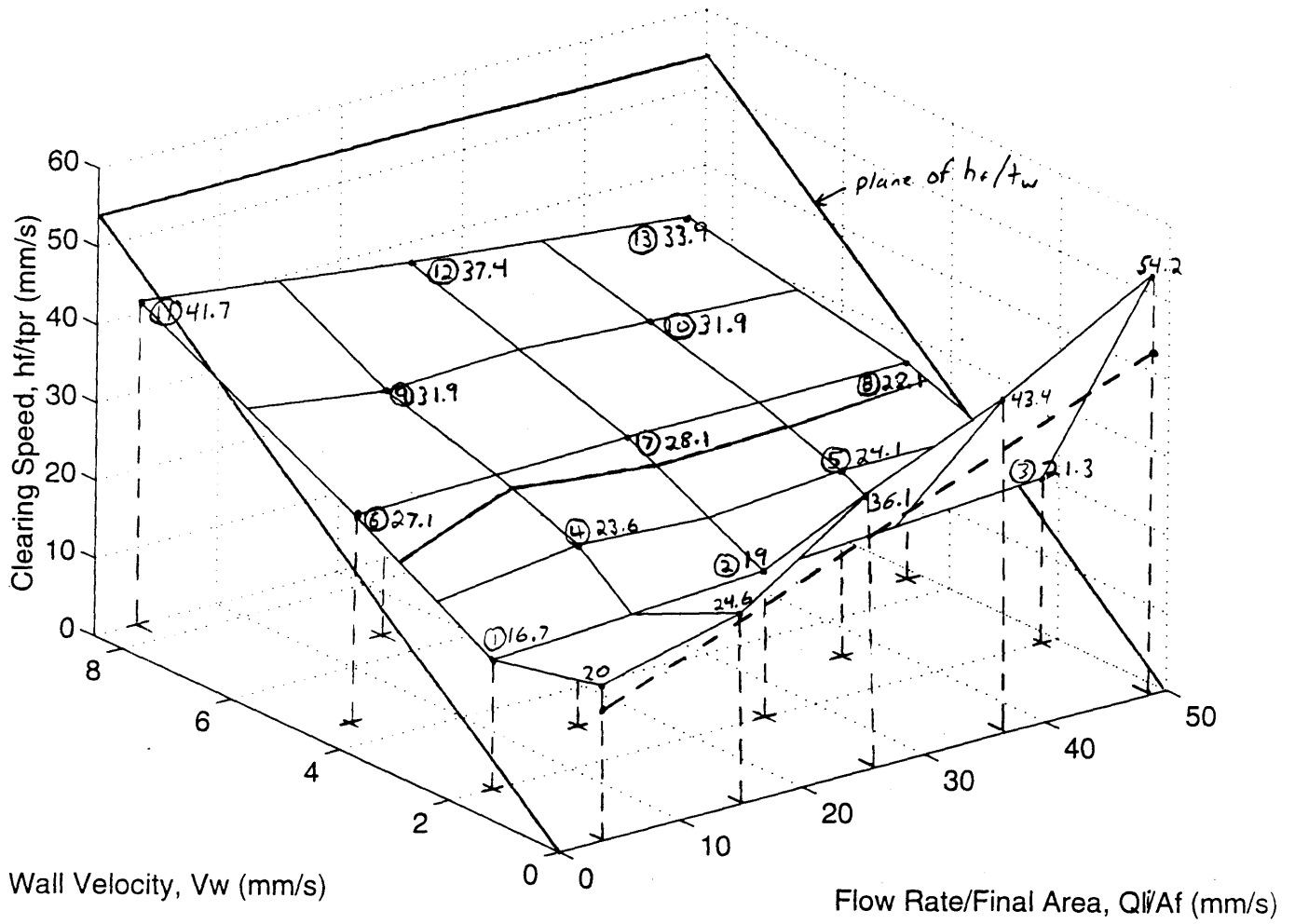


Figure 2-16: Clearing Speed, h_f/t_{pr} .

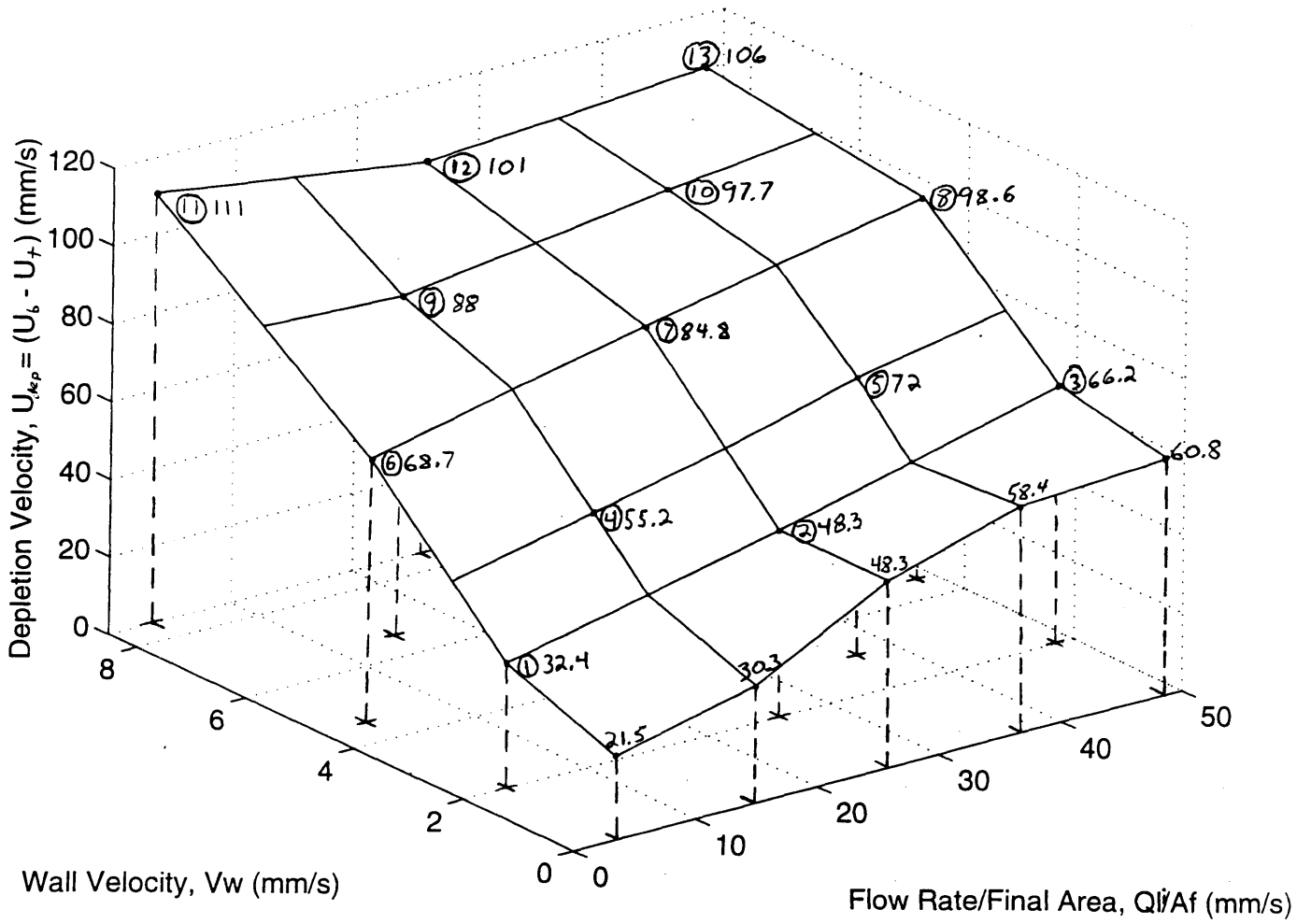


Figure 2-17: Depletion Velocity of Plug.

for very low wall velocities, U_t has a negative value as the top of the plug immediately drops. U_b is always positive indicating the formation of a pocket or gap beneath the plug. The higher Clearing Speed is due primarily to the fact that the plug is deformed to a shorter state, and is not due to increased particle percolation through the plug. Particle percolation is negligible as the fine particles move downward along with the coarse particles even when influenced by the outwardly moving wall.

Included on fig. 2-16 with the dependent variable of h_f/t_{pr} , is the plane of h_f/t_w . This plane indicates the experimental tests, 6-13, where wall stopping time, $t_w (=d_w/V_w)$, occurs prior to t_{pr} , a measurement of the time when the final coarse particles from the broken plug hit the pile of settled coarse. These are tests of interest, because at wall stopping time, t_w , the Fluid Velocity in the test section experiences a sudden jump in value due to the fact that the test section volume is no longer increasing. Further, the jump is more pronounced at the top of the test section where fluid velocity is lower than at the bottom while the chamber volume is increasing. The question is if this jump in Fluid Velocity affects the behavior of the plug, and thus the Clearing Speed. Fig. 2-18 represents Fluid Velocity in Time at various vertical heights in the test section, for test 10, $Q_{li} = 27,000 \text{ mm}^3/\text{s}$ and $V_w = 6.5 \text{ mm/s}$. Also shown are critical time, t_{cr} , process time, t_{pr} , and wall stopping time, t_w . From fig. 2-18, the Fluid Velocity at 100 mm, the approximate initial bed height, jumps from 1.4 mm/s to 37.5 mm/s at $t_w = 1.3$ seconds. The equation for the Fluid Velocity is determined from continuity in a chamber with a constant inlet volume flow rate, and having an outwardly moving wall, fig. 2-19. The velocities are superficial fluid velocities as no account is made in this analysis for the presence of the particle mixture. For a volume of liquid given by eqn. (2.1) where w is the test section width, y is the vertical height of the volume element, and $(d_g + x)$ is its thickness,

$$V = (wy)(d_g + x) \quad (2.1)$$

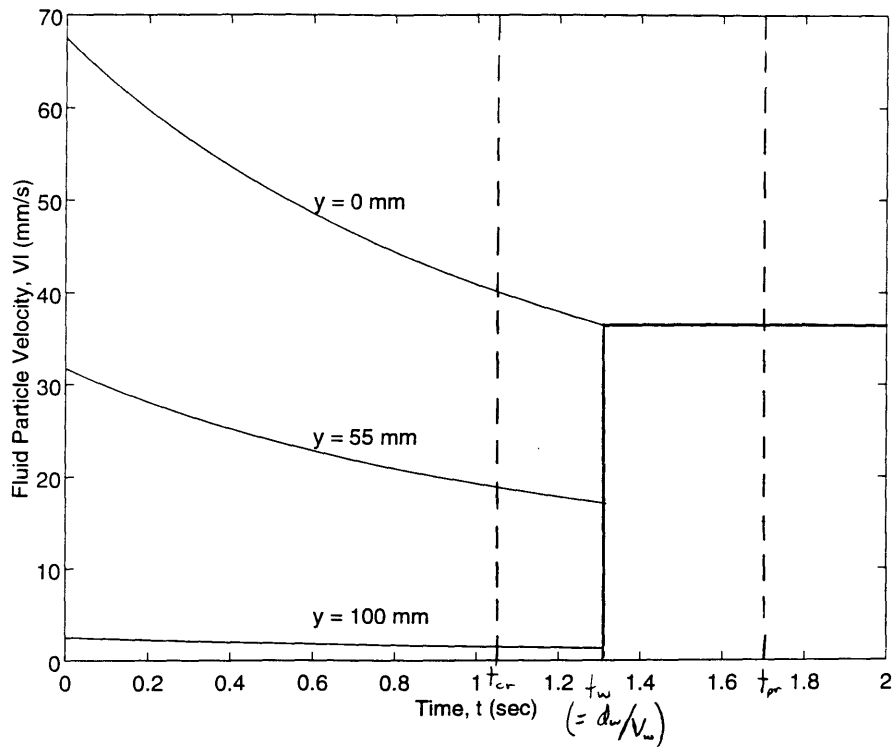


Figure 2-18: Fluid Velocity for Point 10: $Q_{li} = 27,000 \text{ mm}^3/\text{s}$, $V_w = 6.5 \text{ mm/s}$.

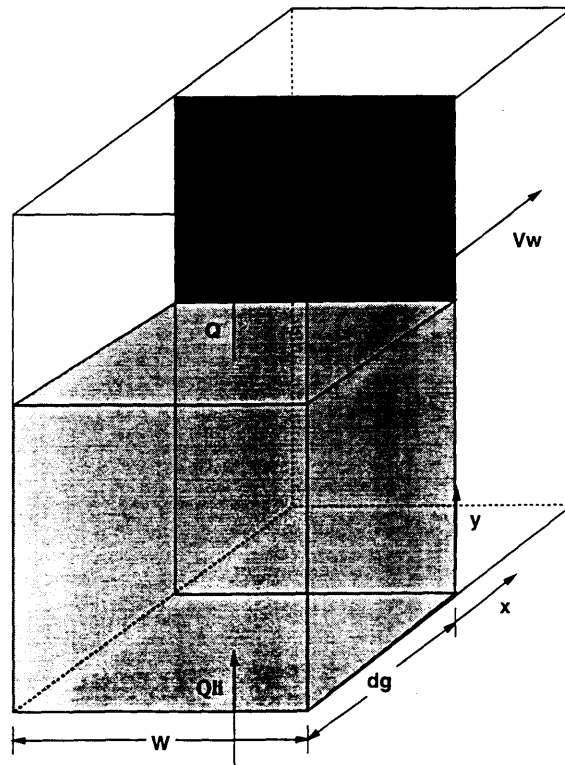


Figure 2-19: Control Volume for Fluid Velocity Analysis.

By continuity, eqn. (2.2) is obtained:

$$\frac{dV}{dt} = (wyV_w) = Q_{li} - Q \quad (2.2)$$

Q_{li} is the Inlet Flow Rate to the volume element, and Q is the outlet flow rate from the volume element. Combining eqn. (2.2) with the definition given below in eqn. (2.3),

$$V_l = \frac{Q}{(w)(d_g + x)} = \frac{Q}{(w)(d_g + V_w t)} \quad (2.3)$$

the following is obtained:

$$V_l(y, t) = \frac{Q_{li} - (wyV_w)}{w(d_g + V_w t)} \quad (2.4)$$

This is the Fluid Velocity equation, a spatial and temporal function, plotted in fig. 2-18. It can be integrated again to determine the vertical position of a fluid particle. With the initial condition of $y(t=0)=0$,

$$y(t) = \frac{Q_{li} t}{w(d_g + V_w t)} \quad (2.5)$$

A plot of this for test 10 is shown in fig. 2-20.

For tests 6-11, the jump in Fluid Velocity occurs after critical breakage time, t_{cr} , and before process time, t_{pr} . This is when the remaining coarse of the broken plug are raining downward. For tests 12 and 13, the jump occurs before both t_{cr} and t_{pr} . This is before plug breakage. The question posed is if the shown step in Fluid Velocity affects the raining speed of the coarse particles. The answer to the question is that an inaccuracy in measuring the Clearing Speed may be obtained if this jump at t_w occurs prior to t_{cr} , the critical plug breakage time. If the jump at t_w occurs after t_{cr} and before t_{pr} , however, measured Clearing Speed should be accurate, because that higher velocity is ordinarily on the order of one-tenth the terminal velocity of the 3.0 mm coarse. t_w consistently occurs between t_{cr} and t_{pr} in time for points 6 - 11, so Clearing Speed is accurate for these points. For points 12 and 13, where t_{cr} occurs prior to t_w , this effect will probably be small if anything at all because t_{cr} and t_w are nearly the same. This is illustrated in fig. 2-21, a plot of the important Events

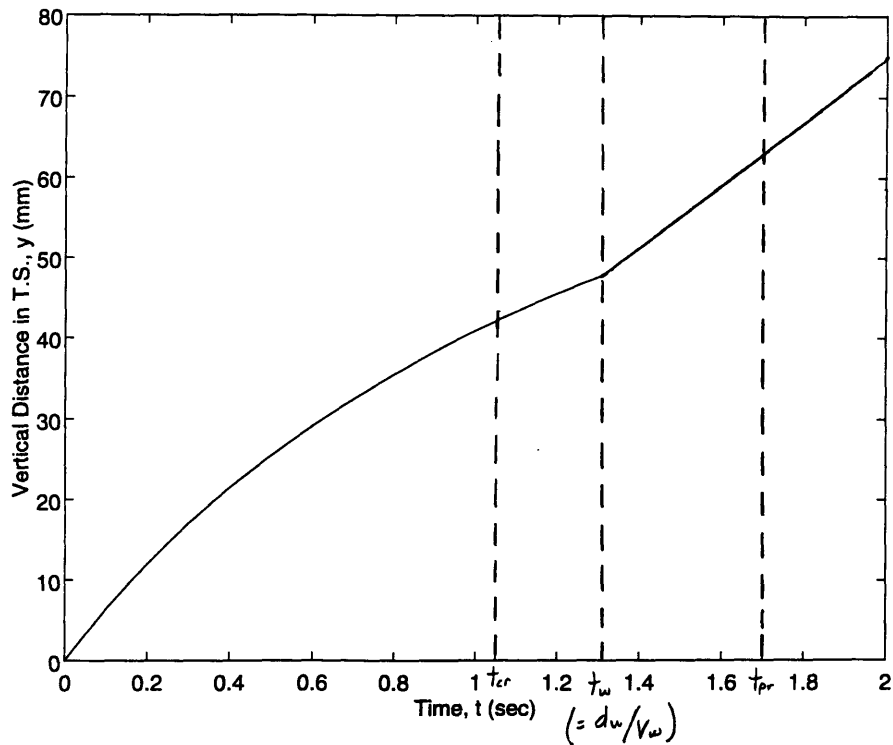


Figure 2-20: Path of Fluid Particle for Point 10: $Q_{li} = 27,000 \text{ mm}^3/\text{s}$, $V_w = 6.5 \text{ mm/s}$.

Occuring in Time for each test: t_* , t_{cr} , t_{pr} , and t_w . t_{cr} , t_{pr} , and t_w are previously defined. t_* (of approximately 1.35 seconds) refers to the time of the “kink” - when flow rate in the test section jumps suddenly as determined from the Step Flow and Step Wall Curve, fig. 2-12. That is , a “pocket” or compliance in the test section absorbs some of the flow until t_* . After t_* , the outlet flow rate has a step to it. t_* was measured from the Step Flow and Step Wall Curve at a given Inlet Flow Rate of $Q_{li} = 31,500 \text{ mm}^3/\text{s}$ and Wall Velocity of $V_w = 2.2 \text{ mm/s}$. It could differ for other Q_{li} , V_w combinations. Interestingly, the jump in outlet superficial liquid velocity at $t_* = 1.35$ seconds was determined to be from 14 mm/s to 30.6 mm/s . The jump in Fluid Velocity for the previously discussed point 10, Inlet Flow Rate, $Q_{li} = 27,000 \text{ mm}^3/\text{s}$ and Wall Velocity, $V_w = 6.5 \text{ mm/s}$, at the approximate initial bed height, 100 mm , was calculated to be from 1.4 mm/s to 37.5 mm/s at $t_w = 1.3$ seconds.

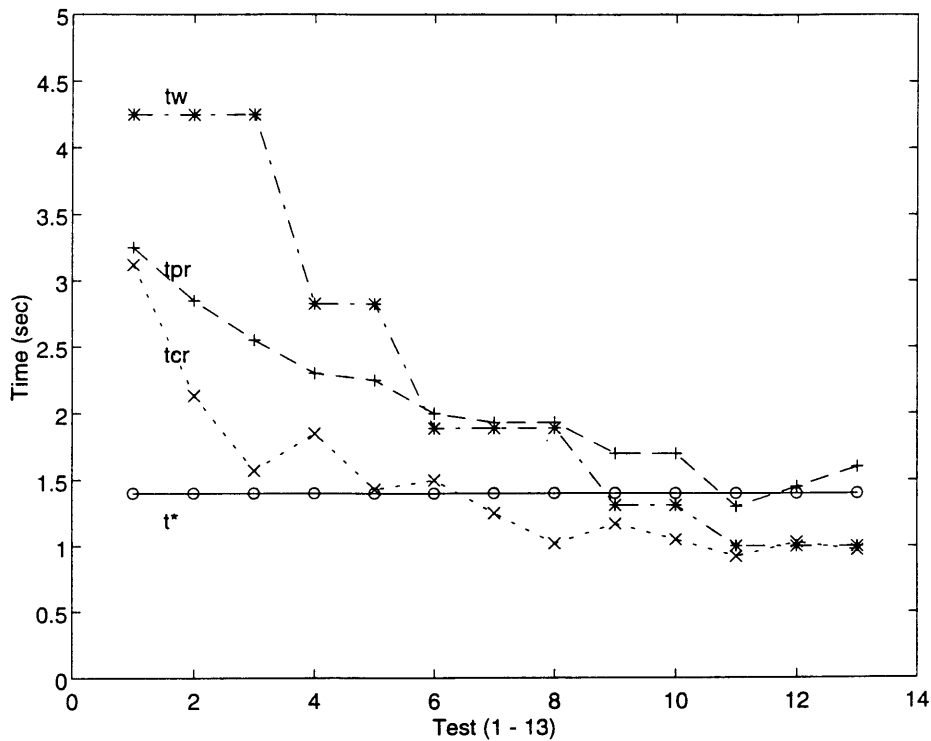


Figure 2-21: Events Occuring in Time.

2.7.3 Fines Removal Fraction at t_{pr}

Fig. 2-22 shows Fines Removal Fraction at process time, t_{pr} , as a function of Wall Velocity, V_w , and Final Superficial Fluid Velocity (Inlet Flow Rate divided by final test section cross-sectional area), Q_{li}/A_f . Once again, it is clear that the five points at zero wall velocity follow Schiaffino's results of Fines Removal in a constant cross-sectional area test section shown in fig. 1-21. A dashed line corresponding to Schiaffino's results is drawn in fig. 2-22. Schiaffino's data revealed that Fines Removal Fraction improves dramatically with liquid superficial velocity, j_l , at velocities above an intermediate point which is approximately $j_l = U_\infty$ (fines terminal velocity). This is true as well with fig. 2-22 which indicates the location of $j_l = U_\infty$. All of the 18 tests follow this trend of sudden improvement in fines removal at this velocity, so it can be concluded that the dominant mechanism in a good Fines Removal Fraction is a liquid superficial velocity that is equal to or higher than the fines terminal velocity U_∞ . The increased wall velocity has no strong effect on the Fines Removal Fraction, although Fines

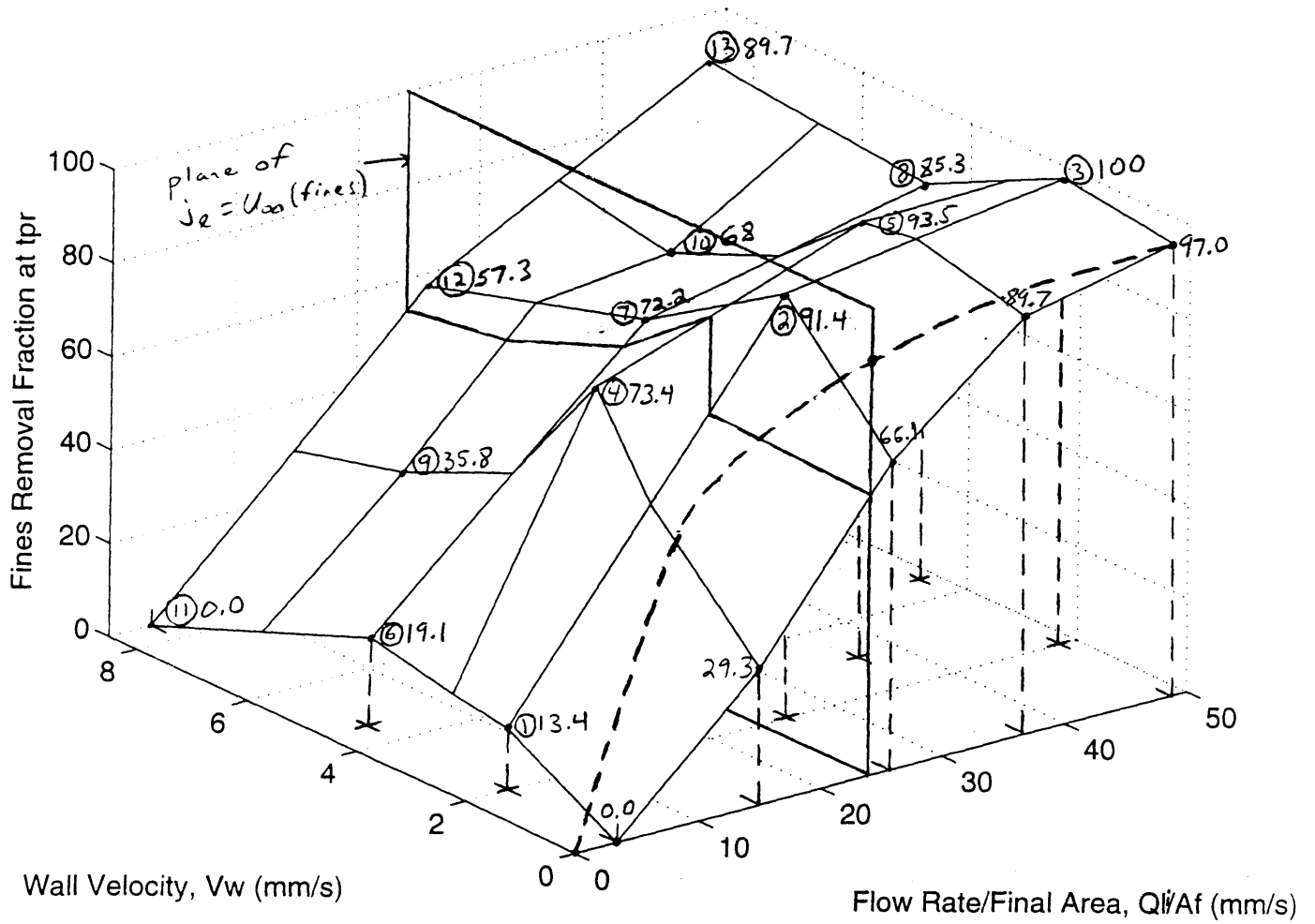


Figure 2-22: Fines Removal Fraction at t_{pr} .

Removal Fraction seems to be the best at the particular Wall Velocity of $V_w = 2.0$ mm/s. This may be because opening the test section just a little relieves the interparticle forces and plug-side wall friction forces favorably. Also, this particular wall velocity may open the plug enough to allow liquid flow to jet through the interstices of the plug, sweeping out fine particles in the most favorable way. At higher wall velocities than 2.0 mm/s, there may be too much jostling of the fine particles or interparticle interaction with the coarse particles in the plug and thus the fines may be in some way be inhibited from being removed. At lower wall velocities than 2.0 mm/s, the fines remain fixed solidly in the plug, and removal is poorer, so some wall movement appears to be beneficial in fines removal.

2.7.4 Maximum Height of Process

Fig. 2-23 shows Maximum Height of the fluidized mechanical segregation process versus Wall Velocity, V_w , and Final Superficial Fluid Velocity (Inlet Flow Rate divided by final cross-sectional area), Q_{fi}/A_f . This plot has no points at zero wall velocity. Fig. 2-23 indicates the plane which separates rising plugs from those that either remain stationary or decrease in height, as explained earlier. In a majority of the 13 tests shown, the maximum height is the original height of the bed, h_o or 98 mm. This is because the superficial fluid velocities are not high enough to raise the plug in the presence of outwardly moving walls. For design of the crushing machine, this is a plus: the less clearance height necessary, the shorter the crushing chamber need be and the less the tendency to discharge coarse material. What actually occurs in the plug upon starting the fluid velocity and wall motion simultaneously is revealed by side view images of the experiments. They show the mixture in the plug tends to flow laterally, filling the volume created by the moving wall. There is no flow channeling through the plug.

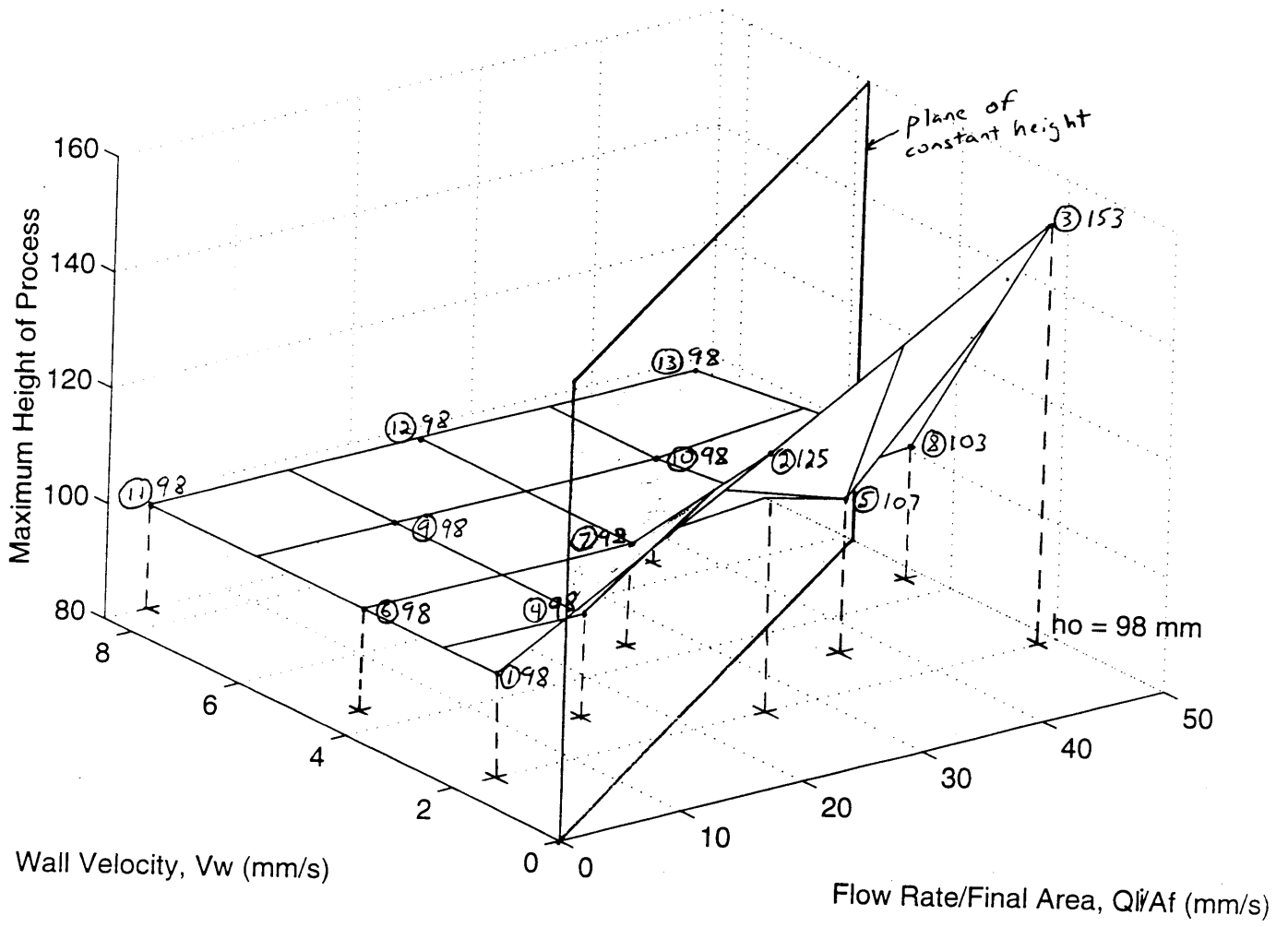


Figure 2-23: Maximum Height of Process.

2.7.5 Best Operating Point: 13

Considering all three design criteria, the best operating point in these tests is probably that at 13, having the highest Inlet Flow Rate ($Q_{li} = 36,000 \text{ mm}^3/\text{s}$) and the highest Wall Velocity ($V_w = 8.5 \text{ mm/s}$). Here, Clearing Speed, h_f/t_{pr} , is near the best of the tests at 33.9 mm/s , as is Fines Removal Fraction at 89.7% . Maximum Height of the Process is the original height of the bed, h_o , because the mixture drops.

The limited testing shows a continuing improvement in the direction of higher fluid flow rates and higher wall velocities. Therefore, these are not necessarily the best design parameters and perhaps further tests should be performed at higher fluid flow rates and higher wall velocities. Given more time on the project, this could be done. It is likely that at higher fluid flow rates and higher wall velocities, even more satisfying results of the design-criterion would be obtained.

Chapter 3

Conclusions

3.1 Summary

The goal of the Comminution Program is to design a comminution machine, incorporating crushing and material transport working together in a cyclical process which would lead to improved comminution efficiencies. The thinking behind this is that in removing fine particles in the interstices of the crushed products by way of material transport, the energy necessary to crush again is significantly reduced. This is because the blunting action of the force is gone when the fines are removed. This study, “Impulsive Segregation of a Bi-Disperse Mixture Between Outwardly Moving Walls”, is only a portion of the research project. Previous research in the program has focused on particle fracture in beds under a compressive load, and two types of fluidization of a bi-disperse mixture of glass beads. Steady fluidization tests of fine particles in a fixed bed of coarse particles were performed and improved experimental correlations were developed for this test. Impulsive fluidization tests on the mixture were performed to understand one of the simplest methods of fine particle removal in the crushing device. In this work, the added complexity of an outwardly moving wall is added to the impulsively fluidized fine particle removal process.

3.1.1 Impulsive Segregation of a Bi-Disperse Mixture Between Outwardly Moving Walls

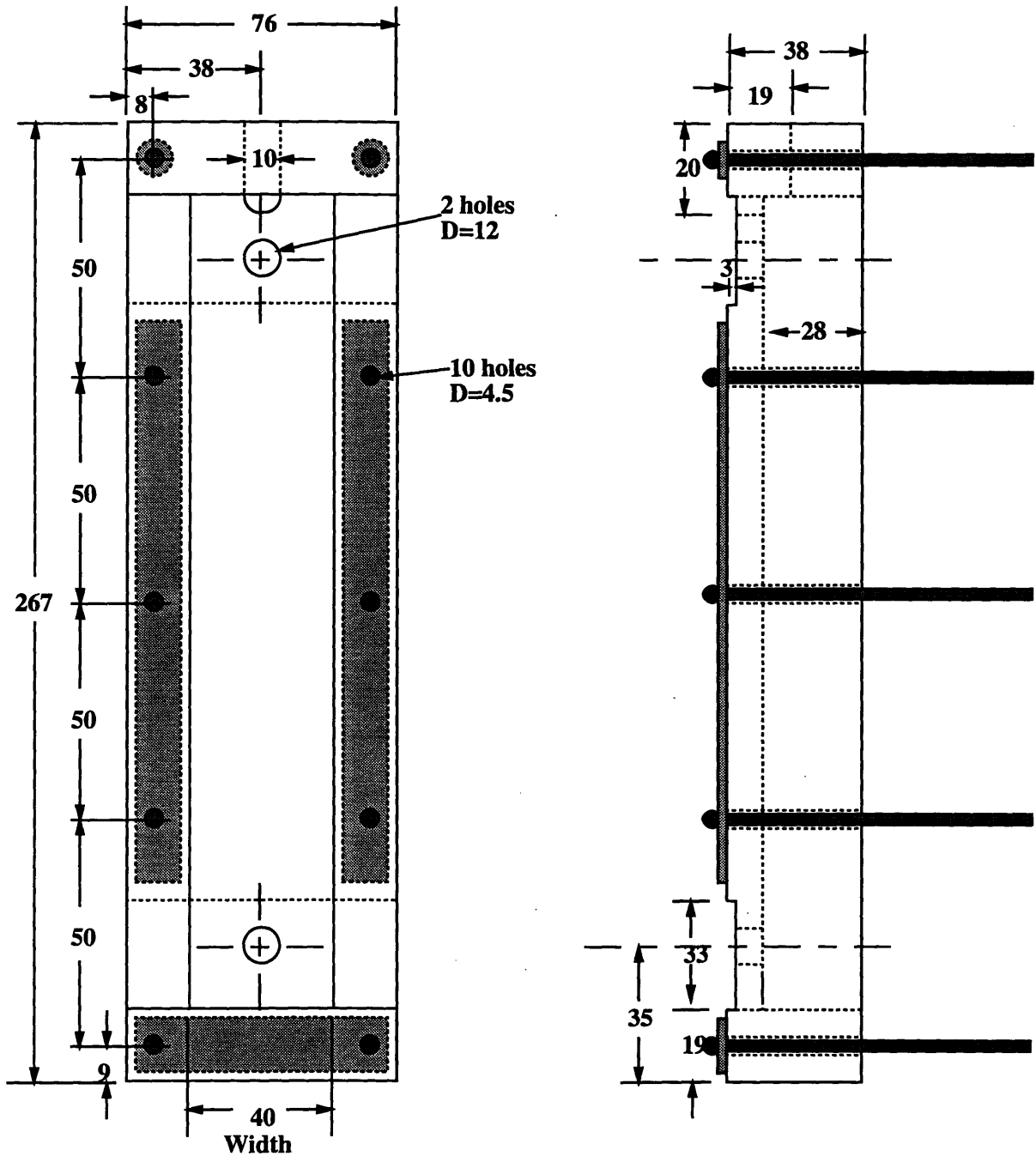
This experimental work is designed to investigate the portion of the crushing machine where the inner member of the crushing device moves away from the outer containing shell, and the crushed material is subject simultaneously to an upward flow and outward wall motion. Observed in these experiments is the formation of a plug which either lifts or drops according to the relative strengths of Inlet Flow Rate and Wall Velocity. Segregation occurs primarily in a pocket of liquid flow underneath the plug where coarse particles rain downwards, and fine particles remain fluidized. The two parameters varied are Inlet Flow Rate and Wall Velocity as these best characterize this fluidized mechanical segregation process. Three three-dimensional plots are created, illustrating three design-criteria as dependent variables, and with Final Superficial Fluid Velocity (Inlet Flow Rate divided by cross-sectional area), Q_{li}/A_f , and Wall Velocity, V_w , combinations serving as the independent variables. Image analysis tools were used to measure the performance. Conclusions from the plots show that the best design point within these tests was at the highest observed Inlet Flow Rate and Wall Velocity. Also, in general, Clearing Speed improved with higher wall velocities, and Fines Removal Fraction improved with inlet flow rate. In some instances, the Maximum Process Height was the original height of the bed.

3.2 Future Work

A more complicated removal process, similar to that which is expected in the actual crushing device, needs to be investigated. A plexiglass test section of a nutating cylinder in an outer cylinder with a bi-disperse mixture held between and subject to liquid jets, is currently being built (Bilimoria, 1994). This will be useful for exploring experimentally the complex, three-dimensional, unsteady physical segregation phenomenon associated with an upward flow through a bi-disperse mixture between eccentric cylinders. The design and construction of such a test section pose many

challenges, but experimental results from such a work will undoubtedly prove valuable to the Comminution Program.

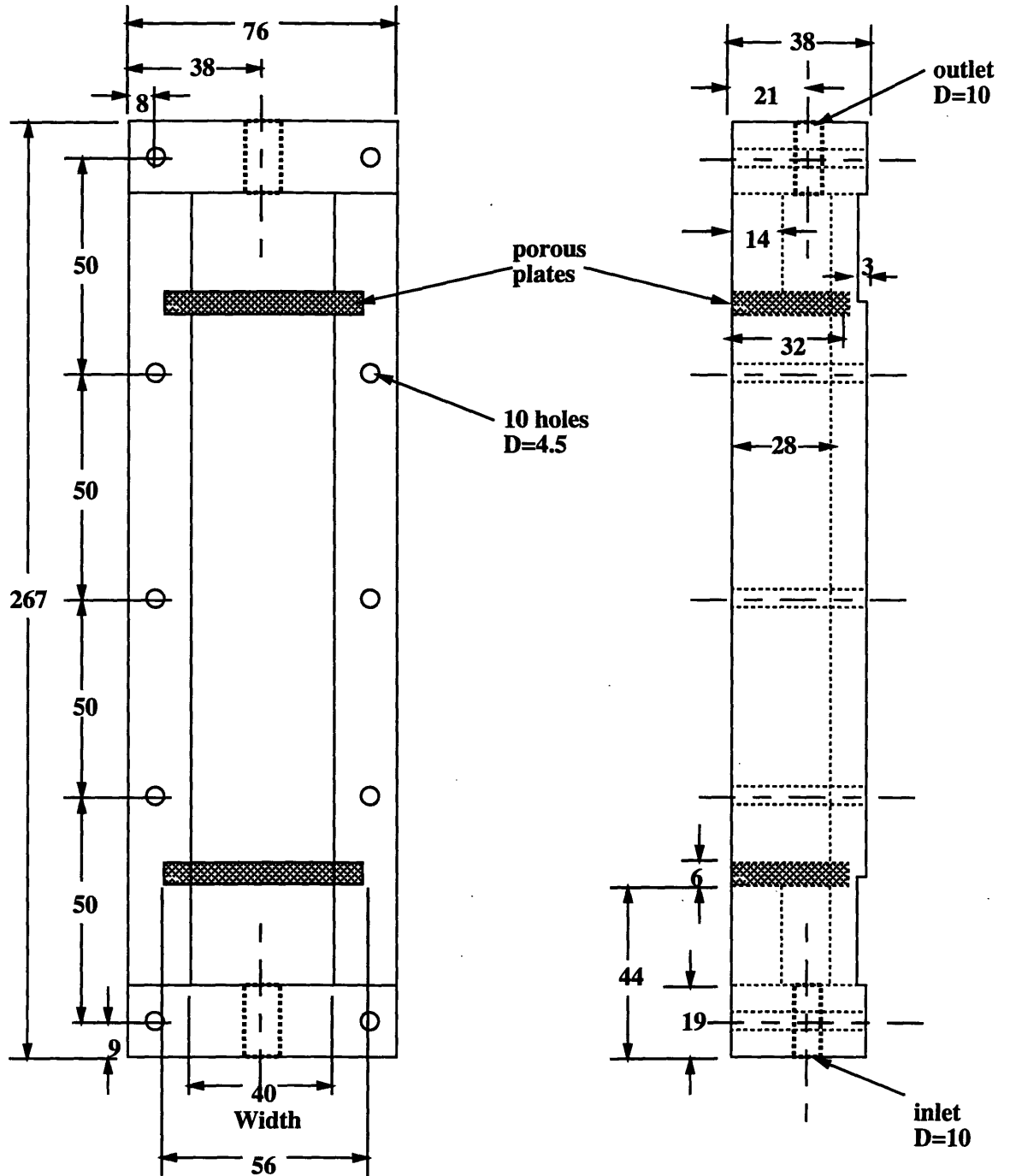
Appendix A: Dimensioned Plexiglass Test Section and Movable Wall



**Inner View of Test Section
(left half)**

**Side View of Test Section
(left half)**

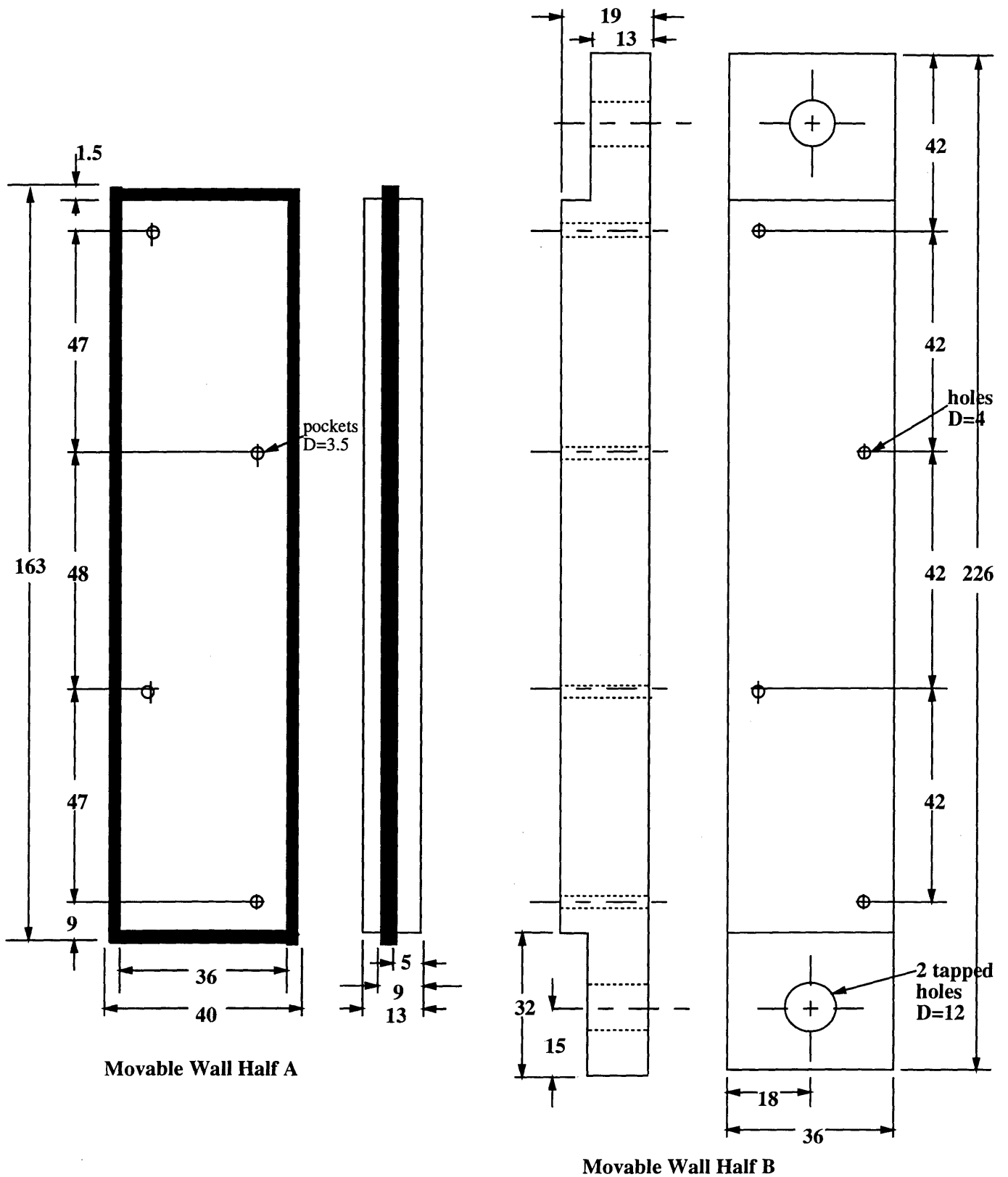
**Note: all dimensions are in mm. Where not specified,
dimensions are assumed to be symmetric.**



**Inner View of Test Section
(right half)**

**Side View of Test Section
(right half)**

Note: all dimensions are in mm. Where not specified, dimensions are assumed to be symmetric.



Note: all dimensions are in mm. Where not specified, dimensions are assumed to be symmetric.

Bibliography

- [1] K. Annis. Segregation control of binary size particles in a comminution device. Master's thesis, Massachusetts Institute of Technology, 1991.
- [2] A.B. Cummins. *Mining Engineering Handbook*. Society of Mining Engineering, 1973.
- [3] A. Frankel, N.A. & Acrivos. On the viscosity of a concentrated suspension of solid spheres. *Chemical Engineering Science*, 22:847–853, 1967.
- [4] C.K. Ghaddar. Fracture efficiency within particle beds. Master's thesis, Massachusetts Institute of Technology, 1991.
- [5] A.D. Kurfess. Fracture criterion for brittle and plastic spheres. Master's thesis, Massachusetts Institute of Technology, 1989.
- [6] H.K. Kytömaa. Viscous particle interactions and their effect on kinematic wave propagation. *Chem. Eng. Comm.*, 105:27–42, 1991.
- [7] K.M. Laffey. Fracture within particle beds under compressive loading. Master's thesis, Massachusetts Institute of Technology, 1987.
- [8] A. Larson. The effect of size and contact geometry in single particle crushing. Master's thesis, Massachusetts Institute of Technology, 1986.
- [9] R.K. McGeary. Mechanical packing of spherical particles. *J. Am. Ceram. Soc.*, pages 513–522, 1961.

- [10] S.D. Misra. Particle breakage and material transport in the design of high-efficiency comminution device. Master's thesis, Massachusetts Institute of Technology, 1991.
- [11] R.B. Mular, A.L. & Bhappu. *Mineral Processing Plant Design*. Society of Mining Engineering, 1980.
- [12] NSF-DOE Workshop. *Flow of Particulates and Fluids*, Gaithersburg, MD, 1990.
- [13] J. Pflueger. The behavior of particle beds in simulation. Master's thesis, Massachusetts Institute of Technology, 1988.
- [14] G.B. Wallis. *One-dimensional Two-Phase Flow*. McGraw-Hill, 1969.